2 ATLAS+CMS DARK MATTER FORUM RECOMMENDA-
3 TIONS

4   Author/contributor list to be added as document is finalized.

1
Introduction

This is a citation test [HK11].

2
Overall choices for simplified models

General topics:

- choice of Dark Matter type: Dirac (unless specified otherwise) and what we might be missing
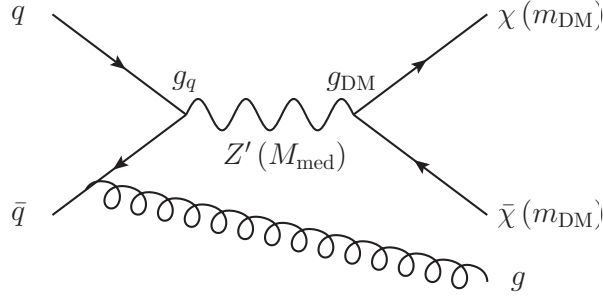
- MFV and what we might be missing

Figure 3.1: The diagram shows the pair production of dark matter particles in association with a parton from the initial state via an s-channel vector or axial-vector mediator. The process if specified by $(M_{\mathrm{med}}, m_{\mathrm{DM}}, g_{\mathrm{DM}}, g_{\mathrm{q}})$, the mediator and dark matter masses, and the mediator couplings to dark matter and quarks respectively.

3

Recommended models for all MET+X analyses

3.1 Vector and axial vector mediator, s-channel exchange

There are several matrix element implementations of the s-channel vector mediated DM production. This is available in POWHEG, MADGRAPH and also MCFM. The implementation in POWHEG generates DM pair production with 1 parton at next-to-leading order (NLO), whilst MADGRAPH and MCFM are at leading order (LO). As shown in POWHEG Ref. [HKR13], including NLO corrections result in an enhancement in the cross section as compared to LO and though this is not significant, it does lead to a substantial reduction in the dependence on the choice of the renormalization and factorization scale and hence the theoretical uncertainty on the signal prediction. Since NLO calculations are available for the process in POWHEG, we recommend to proceed with POWHEG as the generator of choice.

We consider the case of a dark matter particle that is a Dirac fermion and where the production proceeds via the exchange of a spin-1 s-channel mediator. We consider the following interactions between the DM and SM fields including a vector mediator with:

(a) vector couplings to DM and SM,

(b) axial-vector couplings to DM and SM.

The corresponding Lagrangians are

$$\mathcal{L}_{\text{vector}} = \sum_q g_q Z'_\mu \bar{q} \gamma^\mu q + g_{\text{DM}} Z'_\mu \bar{\chi} \gamma^\mu \chi \tag{3.1}$$

$$\mathcal{L}_{\text{axial-vector}} = \sum_q g_q Z'_\mu \bar{q} \gamma^\mu \gamma^5 q + g_{\text{DM}} Z'_\mu \bar{\chi} \gamma^\mu \gamma^5 \chi \tag{3.2}$$

where the coupling extends over all the quarks and universal couplings are assumed for all the quarks. It is also possible to consider another model in which mixed vector and axial-vector couplings are considered, for instance the couplings to the quarks are vector whereas those to DM are axial-vector. As a starting point, we consider only the models with the vector couplings only and axial vector couplings only.

We assume that no additional visible or invisible decays contribute to the width of the mediator, this is referred to as the minimal width and it is defined as follows for the vector and axial-vector models.

$$\Gamma_{\text{min}} = \Gamma_{\bar{\chi}\chi} + \sum_q \Gamma_{\bar{q}q} \tag{3.3}$$

where the individual contributions to this from the partial width are from

$$\Gamma^{\text{V}}_{\bar{\chi}\chi} = \frac{g^2_{\text{DM}} M_{\text{med}}}{12\pi} \left(1 + \frac{2m^2_{\text{DM}}}{M^2_{\text{med}}}\right) \sqrt{1 - \frac{4m^2_{\text{DM}}}{M^2_{\text{med}}}} \tag{3.4}$$

$$\Gamma^{\text{V}}_{\bar{q}q} = \frac{3g^2_q M_{\text{med}}}{12\pi} \left(1 + \frac{2m^2_q}{M^2_{\text{med}}}\right) \sqrt{1 - \frac{4m^2_q}{M^2_{\text{med}}}} \tag{3.5}$$

$$\Gamma^{\text{A}}_{\bar{\chi}\chi} = \frac{g^2_{\text{DM}} M_{\text{med}}}{12\pi} \left(1 - \frac{4m^2_{\text{DM}}}{M^2_{\text{med}}}\right)^{3/2} \tag{3.6}$$

$$\Gamma^{\text{A}}_{\bar{q}q} = \frac{3g^2_q M_{\text{med}}}{12\pi} \left(1 - \frac{4m^2_q}{M^2_{\text{med}}}\right)^{3/2}. \tag{3.7}$$

Note the color factor 3 in the quark terms. Figure 3.2 shows the minimal width as a function of mediator mass for both vector and axial-vector mediators assuming couplings of 1. With this choice of the couplings, the dominant contribution to the minimal width comes from the quarks due to the color factor enhancement.

The simplified models described here have four free parameters: mediator mass M_{med}, Dark Matter mass m_{DM}, coupling of the mediator to quarks g_q and coupling of the mediator to Dark Matter g_{DM}. In order to determine an optimal choice of the parameter grid for presentation of the early Run-2 results, dependencies of the kinematic quantities and cross sections on the individual parameters need to be studied. The following paragraphs list the main observations from
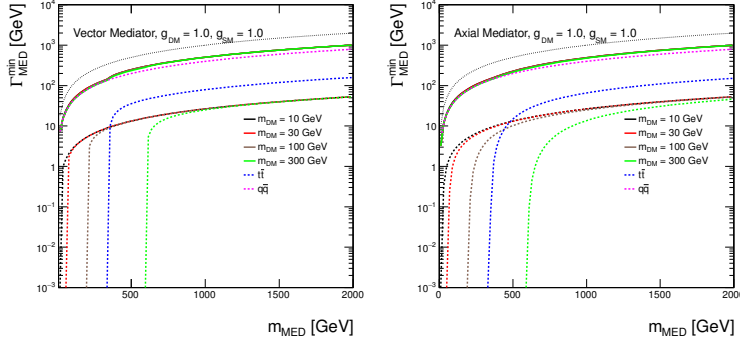
Figure 3.2: Minimal width as a function of mediator mass for vector and axial-vector mediator assuming couplings of 1. The total width is shown as solid lines for Dark Matter masses of 10 GeV, 30 GeV, 100 GeV and 300 GeV in black, red, brown and green, respectively. The individual contributions from Dark Matter are indicated by dotted lines with the same colors. The contribution from all quarks but top is shown as magenta dotted line and the contribution from top quarks only is illustrated by the dotted blue line. The dotted black line shows the extreme case $\Gamma_{\min} = M_{\mathrm{med}}$.

61 the scans over the parameters that support the final proposal for the
62 parameter grid.

63 *Scan over the couplings* Figure 3.3 reveals there are no differences in
64 the shape of the $\not{E}_T$ distribution among the samples where the pair of
65 10 GeV Dark Matter particles are produced on-shell from the media-
66 tor of 1 TeV, generated with different choice of the coupling strength.
67 The considered coupling values range from 0.1 to 1.45, where the
68 latter value approximates the maximum allowed coupling value,
69 holding $g_q = g_{\mathrm{DM}}$, such that $\Gamma_{\min} < M_{\mathrm{med}}$. Based on similar plots for
70 different choices of mediator and Dark Matter masses, it is concluded
71 that the shapes of kinematic distributions are not altered neither for
72 the on-shell Dark Matter production where $M_{\mathrm{med}} > 2m_{\mathrm{DM}}$, nor for
73 the off-shell Dark Matter production where $M_{\mathrm{med}} < 2m_{\mathrm{DM}}$. Only
74 the cross sections change. Differences in kinematic distributions are
75 expected only close to the transition region where both on-shell and
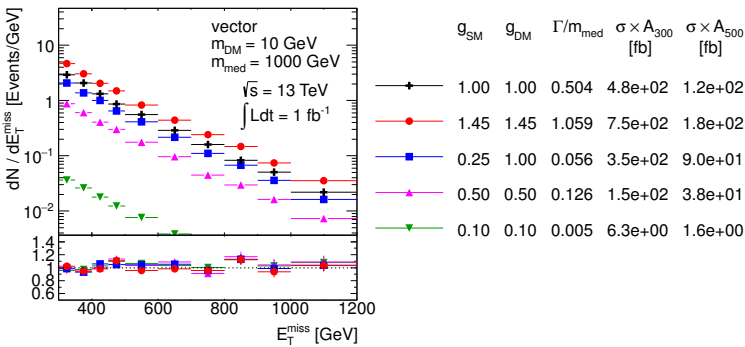off-shell regimes mix.

Figure 3.3: Scan over couplings. The $\not{E}_T$ distribution is compared for the vector mediator models using the parameters as indicated. Ratios of the normalized distributions with respect to the first one are shown. A_{300} and A_{500} in the table denote the acceptance of the $\not{E}_T > 300$ GeV and $\not{E}_T > 500$ GeV cut, respectively.

76
77 The only place where special care needs to be taken are extremely
78 heavy and narrow mediators, in other words with low couplings.
79 Figure 3.4 suggests a change in the shape of the $\not{E}_T$ distribution for
80 5 TeV mediator once $\Gamma_{\min}/M_{\mathrm{med}}$ gets down to the order of percent or

below. This, however, does not come from physics as it is a feature of
the generator implementation, where a cutoff for the regions far away
from the mediator mass is often used. This is illustrated in Fig. 3.5
showing the invariant mass of the Dark Matter pair in the samples
generated for 7 TeV mediator with different coupling strength. In
all cases, it is expected to observe a peak around the mediator mass
with a tail extending to $m_{\bar{\chi}\chi} \to 0$, significantly enhanced by parton
distribution functions at low Bjorken x. For coupling strength 1 and
3, the massive enhancement at $m_{\bar{\chi}\chi} \to 0$ implies the resonant pro-
duction at $m_{\bar{\chi}\chi} = 7$ TeV is statistically suppressed such that barely
any events are generated there. However, for narrower mediators
with couplings below 1, the peak around 7 TeV is clearly visible in
the generated sample and the dominant tail at $m_{\bar{\chi}\chi} \to 0$ is artificially
cut off, leading to unphysical cross section predictions and kinematic
shapes. This explains why the sample with the narrowest mediator in
Fig. 3.4 is heavily suppressed in terms of production cross section and
also gives different $\not{E}_T$ shape. In general, for such extreme parameter
choices the EFT model should give the correct answer. **[TODO: add
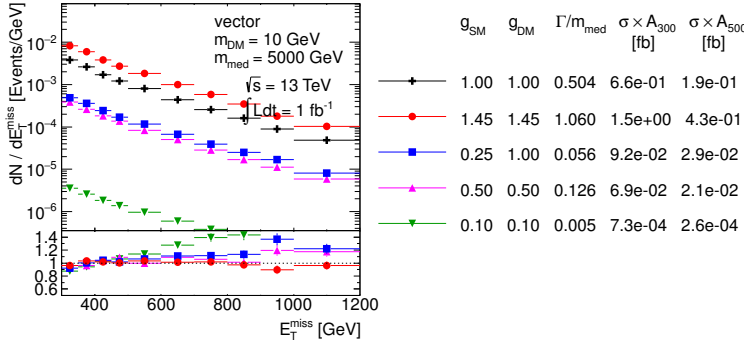results of ongoing study.]**

Figure 3.4: Scan over couplings. The $\not{E}_T$ distribution is compared for the vector mediator models using the parameters as indicated. Ratios of the normalized distributions with respect to the first one are shown. A_{300} and A_{500} in the table denote the acceptance of the $\not{E}_T > 300$ GeV and $\not{E}_T > 500$ GeV cut, respectively.

Scan over the Dark Matter mass   For the fixed mediator mass and cou-
plings, both the cross section and the kinematic distributions remain
similar for different Dark Matter masses as long as $M_{\mathrm{med}} > 2m_{\mathrm{DM}}$.
This is illustrated in Fig. 3.6 on an example of 1 TeV mediator and
Dark Matter masses ranging from 10 GeV to 300 GeV. It is observed
that the cross section decreases as the Dark Matter mass reaches
closer to $M_{\mathrm{med}}/2$. Once the Dark Matter pair is produced off-shell,
the cross section of such simplified model is suppressed and the $\not{E}_T$
spectrum hardens, as demonstrated with the choice of 1 TeV Dark
Matter in the same plot. Figure 3.7 reveals the $\not{E}_T$ spectrum hardens
further with increasing Dark Matter mass, accompanied by the grad-
ual decrease of the cross section. From these observations one can
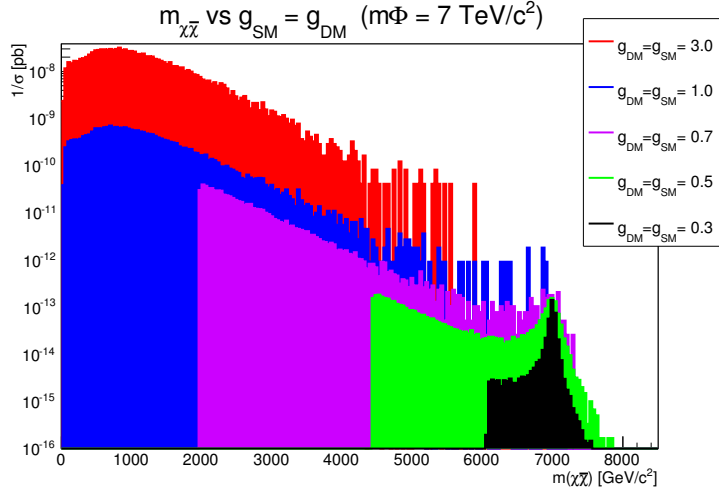conclude:

Figure 3.5: Invariant mass of the Dark Matter pair in the samples with $M_{\mathrm{med}} = 7\,\mathrm{TeV}$ and different coupling strengths.

- A coarse binning along m_{DM} is sufficient at $M_{\mathrm{med}} \gg 2m_{\mathrm{DM}}$.

- Finer binning is needed in order to capture the changes in the cross section and kinematic quantities close to the production threshold on both sides around $M_{\mathrm{med}} = 2m_{\mathrm{DM}}$.

- Due to the significant cross section suppression of the off-shell Dark Matter pair production, it is not necessary to populate the parameter space $M_{\mathrm{med}} \ll 2m_{\mathrm{DM}}$ since the LHC is not going to be able to probe the models there.

Figure 3.6: Scan over Dark Matter mass. The $\not{E}_T$ distribution is compared for the vector mediator models using the parameters as indicated. Ratios of the normalized distributions with respect to the first one are shown. A_{300} and A_{500} in the table denote the acceptance of the $\not{E}_T > 300\,\mathrm{GeV}$ and $\not{E}_T > 500\,\mathrm{GeV}$ cut, respectively.

Scan over the mediator mass   Changing the mediator mass for fixed Dark Matter mass and couplings leads to significant differences in cross section and shapes of the kinematic variables for $M_{\mathrm{med}} > 2m_{\mathrm{DM}}$ as shown in Fig. 3.8. As expected, higher mediator masses lead to harder $\not{E}_T$ spectra. On the other hand, the $\not{E}_T$ shapes are similar in the off-shell Dark Matter production regime as well as no dramatic differences in cross sections are observed, which is illustrated
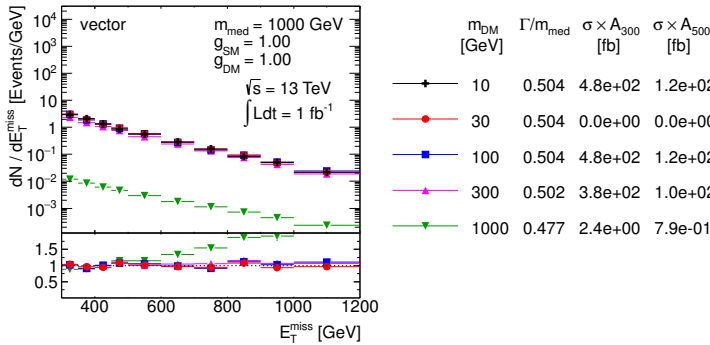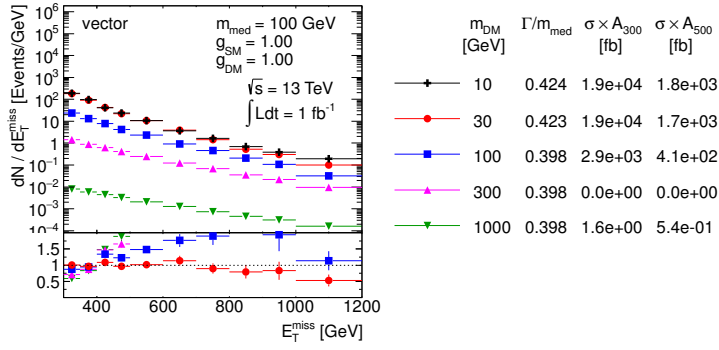
Figure 3.7: Scan over Dark Matter mass. The $\not{E}_T$ distribution is compared for the vector mediator models using the parameters as indicated. Ratios of the normalized distributions with respect to the first one are shown. A_{300} and A_{500} in the table denote the acceptance of the $\not{E}_T > 300\,\text{GeV}$ and $\not{E}_T > 500\,\text{GeV}$ cut, respectively.

in Fig. 3.9. Therefore, a coarse binning along m_{DM} is sufficient at $M_{\text{med}} \ll 2m_{\text{DM}}$.
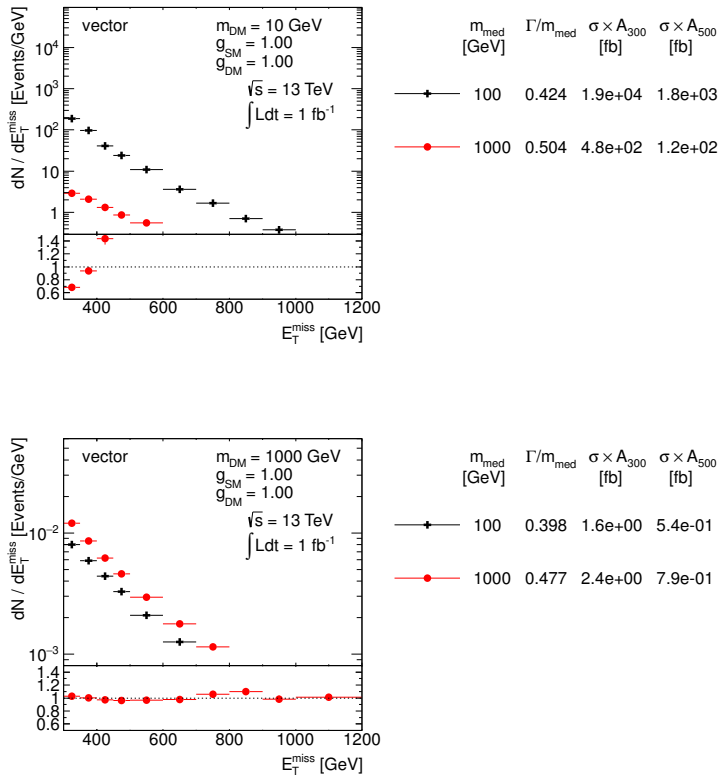
Figure 3.8: Scan over mediator mass. The $\not{E}_T$ distribution is compared for the vector mediator models using the parameters as indicated. Ratios of the normalized distributions with respect to the first one are shown. A_{300} and A_{500} in the table denote the acceptance of the $\not{E}_T > 300\,\text{GeV}$ and $\not{E}_T > 500\,\text{GeV}$ cut, respectively.

Figure 3.9: Scan over mediator mass. The $\not{E}_T$ distribution is compared for the vector mediator models using the parameters as indicated. Ratios of the normalized distributions with respect to the first one are shown. A_{300} and A_{500} in the table denote the acceptance of the $\not{E}_T > 300\,\text{GeV}$ and $\not{E}_T > 500\,\text{GeV}$ cut, respectively.

Proposed parameter grid   Based on the observations above, the following proposal is made for the presentation of the early Run-2 results from the LHC:

(a) Give results in the M_{med}–m_{DM} plane for a particular choice of the couplings.

(b) Give results in the g_q–g_{DM} plane for a particular choice of the masses.

We choose to display the results in the M_{med}–m_{DM} plane for the choice of the couplings $g_{\mathrm{q}} = g_{\mathrm{DM}} = 1$. In order to motivate the highest mediator mass grid point, the expected sensitivity of Run-2 LHC data needs to be taken into account. The expected upper limit at 95% confidence level on the product of cross section, acceptance and efficiency, $\sigma \times A \times \epsilon$, in the final Run-1 ATLAS mono-jet analysis [A$^+$15] is 51 fb and 7.2 fb for $\not{E}_T > 300\,\mathrm{GeV}$ and $\not{E}_T > 500\,\mathrm{GeV}$, respectively. The ATLAS 14 TeV prospects [ATL14] predict twice better sensitivity with the first $5\,\mathrm{fb}^{-1}$ of data already. Given the cross section for $V+$jets processes increases by roughly a factor 2 when going from $\sqrt{s} = 8\,\mathrm{TeV}$ to 13 TeV, similar fiducial cross section limits can be expected with the first Run-2 data as from the final Run-1 analysis. The generator level cross section times the acceptance at $\not{E}_T > 500\,\mathrm{GeV}$ for the model with couplings $g_{\mathrm{q}} = g_{\mathrm{DM}} = 1$, light Dark Matter of 10 GeV and 1 TeV vector mediator is at the order of 100 fb, i.e. the early Run-2 mono-jet analysis is going to be sensitive to heavier mediators than this. The value of $\sigma \times A$ at $\not{E}_T > 500\,\mathrm{GeV}$ for 5 TeV vector mediator is at the order of 0.1 fb, therefore this model probably lies beyond the reach of the LHC. Based on these arguments, the following M_{med} grid points are chosen, roughly equidistant in the logarithmic scale: 10 GeV, 20 GeV, 50 GeV, 100 GeV, 200 GeV, 300 GeV, 500 GeV, 1000 GeV and 2000 GeV. Given the fact that significant changes in cross section happen around the $M_{\mathrm{med}} = 2m_{\mathrm{DM}}$ threshold, the m_{DM} grid points are taken at approximately $M_{\mathrm{med}}/2$, namely: 10 GeV, 50 GeV, 150 GeV, 500 GeV and 1000 GeV. Points on the on-shell diagonal are always chosen to be 5 GeV away from the threshold, to avoid numerical instabilities in the event generation. The detailed studies of the impact of the parameter changes on the cross section and kinematic distributions presented earlier in this section support removing some of the grid points and rely on interpolation. The optimised grids proposed for the vector and axial-vector mediators are given in Table. 3.1, containing 29 mass points each. One point at very high mediator mass (5 TeV) is added for each of the DM masses scanned, to aid the reinterpretation of results in terms of contact interaction operators (EFTs).

m_{DM} (GeV)	m_{med} (GeV)									
1	10	20	50	100	200	300	500	1000	2000	5000
10	10	15	50	100						5000
50	10		50	95	200	300				5000
150	10				200	295	500			5000
500	10						500	995	2000	5000
1000	10							1000	1995	5000

Table 3.1: Simplified model benchmarks for $s-$channel simplified models (spin-1 mediators decaying to Dirac DM fermions in the V and A case, taking the minimum width for $g_{\mathrm{q}} = g_{\mathrm{DM}} = 1$)

The presentation of the results in the g_q–g_{DM} plane for fixed masses benefits from cross section scaling and is discussed in Section 3.3.

3.2 *Scalar and pseudoscalar mediator, s-channel exchange*

One of the most simple UV complete extensions of the effective field theory approach is the addition of a scalar/pseudoscalar mediator between DM and SM. A gauge singlet mediator can have tree-level interactions with a singlet DM particle that is either a Dirac or Majorana fermion, or DM that is a scalar itself. The spin-0 mediator can either be a real or complex scalar; a complex scalar contains both scalar and pseudoscalar particles, whereas the real field only contains the scalar particle. In this document we consider only two of the possible choices for this simplified model: one where the interaction with the SM is mediated by a real scalar, and the second where we consider only a light pseudoscalar, assuming that the associated scalar is decoupled from the low-energy spectrum. The kinematics of the two cases is sufficiently different to suggest that further investigation of the complex scalar case is needed but left for future studies.

Couplings to the SM fermions can be arranged by mixing with the SM Higgs. Such models have interesting connections with Higgs physics, and can be viewed as generalizations of the Higgs portal to DM. The most general scalar mediator models will have renormalizable interactions between the SM Higgs and the new scalar ϕ or pseudoscalar a, as well as ϕ/a interactions with electroweak gauge bosons. Such interactions are model dependent, often subject to constraints from electroweak precision tests, and would suggest specialized searches which cannot be generalized to a broad class of models (unlike, for instance, the $\not{E}_T +$ jets searches). As a result, for this class of minimal simplified models with spin-0 mediators, we will focus primarily on couplings to fermions and loop-induced couplings to gluons.

Minimal Flavor Violation (MFV) implies that scalar couplings to fermions will be proportional to the fermion mass. However, they can differ for up- and down-type quarks and for charged leptons.

Following the assumption that DM is a fermion χ, which couples to the SM only through a scalar ϕ or pseudoscalar a, the most general tree-level Lagrangians compatible with the MFV assumption

210   are [CRTW14, ADR$^+$14, BFG15]:

$$\mathcal{L}_{\text{fermion},\phi} = \mathcal{L}_{\text{SM}} + i\bar{\chi}\not{\partial}\chi + m_\chi\bar{\chi}\chi + |\partial_\mu\phi|^2 + \frac{1}{2}m_\phi^2\phi^2 +$$
$$g_\chi\phi\bar{\chi}\chi + \frac{\phi}{\sqrt{2}}\sum_i\left(g_u y_i^u \bar{u}_i u_i + g_d y_i^d \bar{d}_i d_i + g_\ell y_i^\ell \bar{\ell}_i \ell_i\right), \qquad (3.8)$$

$$\mathcal{L}_{\text{fermion},a} = \mathcal{L}_{\text{SM}} + i\bar{\chi}\not{\partial}\chi + m_\chi\bar{\chi}\chi + |\partial_\mu a|^2 + \frac{1}{2}m_a^2 a^2 +$$
$$ig_\chi a\bar{\chi}\gamma_5\chi + \frac{ia}{\sqrt{2}}\sum_i\left(g_u y_i^u \bar{u}_i\gamma_5 u_i + g_d y_i^d \bar{d}_i\gamma_5 d_i + g_\ell y_i^\ell \bar{\ell}_i\gamma_5\ell_i\right) \quad (3.9)$$

211   Here the sums run over the all SM generations; the Yukawa couplings
212   y_i^f are normalized to $y_i^f = \sqrt{2}m_i^f/v$ where $v \simeq 246\,\text{GeV}$ represents
213   the Higgs vacuum expectation value (VEV). We parametrise the DM-
214   mediator coupling as g_χ, without any additional Yukawa structure
215   between the mediator and the dark sector.
216   As already stated we only choose a minimal set of interactions that
217   do not include interactions with the Higgs field. For simplicity, we
218   also assume universal SM-mediator couplings $g_v = g_u = g_d = g_\ell$
219   Given these simplifications, the minimal set of parameters under
220   consideration is

$$\left\{m_\chi,\ m_{\phi/a},\ g_\chi,\ g_q\right\}. \qquad (3.10)$$

221   The matrix element implementation of the s-channel spin-0 medi-
222   ated DM production is available in POWHEG with the full top-loop
223   calculation at LO [HR15].
        We choose to consider minimal mediator width given by Eq. 3.3,
    where the individual contributions follow from

$$\Gamma_{\bar{\chi}\chi}^S = \frac{g_{\text{DM}}^2 M_{\text{med}}}{8\pi}\left(1 - \frac{4m_{\text{DM}}^2}{M_{\text{med}}^2}\right)^{3/2} \qquad (3.11)$$

$$\Gamma_{\bar{q}q}^S = \frac{3g_q^2 M_{\text{med}}}{8\pi}\frac{m_q^2}{v^2}\left(1 - \frac{4m_q^2}{M_{\text{med}}^2}\right)^{3/2} \qquad (3.12)$$

$$\Gamma_{\bar{\chi}\chi}^P = \frac{g_{\text{DM}}^2 M_{\text{med}}}{8\pi}\sqrt{1 - \frac{4m_{\text{DM}}^2}{M_{\text{med}}^2}} \qquad (3.13)$$

$$\Gamma_{\bar{q}q}^P = \frac{3g_q^2 M_{\text{med}}}{8\pi}\frac{m_q^2}{v^2}\sqrt{1 - \frac{4m_q^2}{M_{\text{med}}^2}}. \qquad (3.14)$$

224   The minimal width for scalar and pseudo-scalar mediators with
225    $g_q = g_{\text{DM}} = 1$ are shown in Fig. 3.10, illustrating the effect of the
226   Higgs-like Yukawa couplings. For the mediator masses above twice
227   the top quark mass m_t, the minimal width receives the dominant
228   contribution from the top quark. For lighter mediator masses, Dark
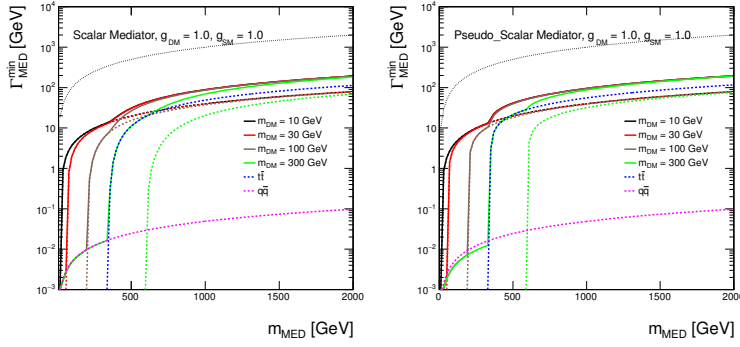229   Matter dominates as the couplings to lighter quarks are Yukawa

Figure 3.10: Minimal width as a function of mediator mass for scalar and pseudo-scalar mediator assuming couplings of 1. The total width is shown as solid lines for Dark Matter masses of 10 GeV, 30 GeV, 100 GeV and 300 GeV in black, red, brown and green, respectively. The individual contributions from Dark Matter are indicated by dotted lines with the same colors. The contribution from all quarks but top is shown as magenta dotted line and the contribution from top quarks only is illustrated by the dotted blue line. The dotted black line shows the extreme case $\Gamma_{\min} = M_{\mathrm{med}}$.

suppressed. Note that we decide to ignore the partial width coming from gluons through loops as it can be safely neglected [HR15].

Similarly as in the case of the vector and axial-vector mediators, scans in the parameter space are performed also for the scalar and pseudo-scalar mediators in order to decide on the optimised parameter grid for the presentation of Run-2 results. Figures 3.11- 3.15 show the scans over the couplings, Dark Matter mass and mediator mass and the same conclusions apply as in Section 3.1.

Since the top quark gives the dominant contribution to the mediator width due to Higgs-like Yukawa couplings, the effect of the top channel opening in the mediator production was studied in addition. Scan over the mediator mass is shown in Fig. 3.15 where the mediator masses 300 GeV and 500 GeV are chosen to be below and above $2m_t$. The off-shell Dark Matter production regime is assumed by taking $m_{\mathrm{DM}} = 1\,\mathrm{TeV}$ in order to allow studying solely the effects of the couplings to quarks. No differences in the kinematic distributions are observed and also the cross sections remain similar in this case. Therefore, it is concluded that no significant changes appear for mediator masses around the $2m_t$ threshold.

Figure 3.11: Scan over couplings. The $\not{E}_T$ distribution is compared for the scalar mediator models using the parameters as indicated. Ratios of the normalized distributions with respect to the first one are shown. A_{300} and A_{500} in the table denote the acceptance of the $\not{E}_T > 300\,\mathrm{GeV}$ and $\not{E}_T > 500\,\mathrm{GeV}$ cut, respectively.

The optimized parameter grid in the M_{med}–m_{DM} plane for scalar and pseudo-scalar mediators is motivated by similar arguments as

m_{DM} [GeV]	Γ/m_{med}	$\sigma \times A_{300}$ [fb]	$\sigma \times A_{500}$ [fb]
10	0.062	3.3e+01	4.0e+00
30	0.061	3.1e+01	4.1e+00
100	0.053	2.5e+01	3.2e+00
300	0.022	1.3e-01	2.6e-02
1000	0.022	3.4e-05	1.2e-05

Figure 3.12: Scan over Dark Matter mass. The $\not{E}_T$ distribution is compared for the scalar mediator models using the parameters as indicated. Ratios of the normalized distributions with respect to the first one are shown. A_{300} and A_{500} in the table denote the acceptance of the $\not{E}_T > 300\,\text{GeV}$ and $\not{E}_T > 500\,\text{GeV}$ cut, respectively.

m_{DM} [GeV]	Γ/m_{med}	$\sigma \times A_{300}$ [fb]	$\sigma \times A_{500}$ [fb]
10	0.037	8.0e+01	7.0e+00
30	0.020	4.5e+01	3.8e+00
100	0.000	1.2e+00	1.5e-01
300	0.000	5.3e-02	1.1e-02
1000	0.000	3.2e-05	1.1e-05

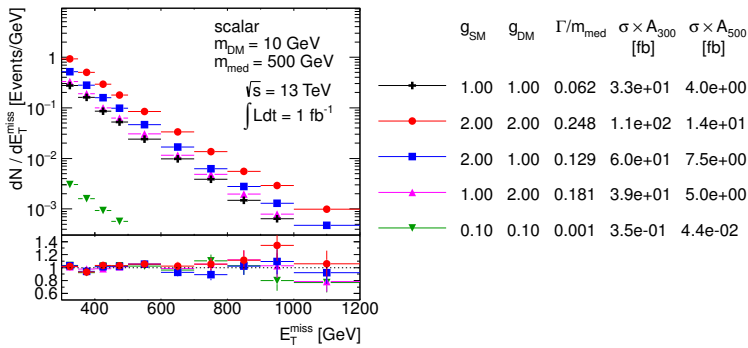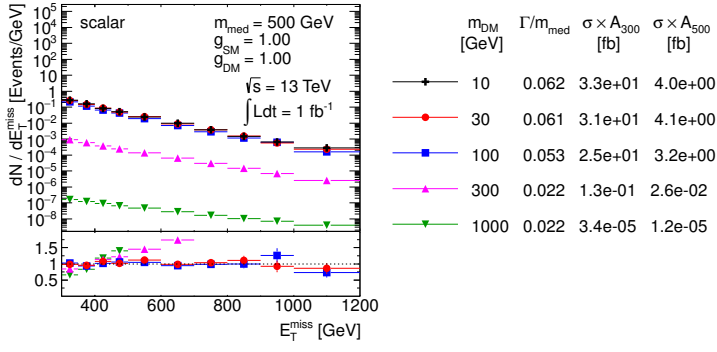Figure 3.13: Scan over Dark Matter mass. The $\not{E}_T$ distribution is compared for the scalar mediator models using the parameters as indicated. Ratios of the normalized distributions with respect to the first one are shown. A_{300} and A_{500} in the table denote the acceptance of the $\not{E}_T > 300\,\text{GeV}$ and $\not{E}_T > 500\,\text{GeV}$ cut, respectively.

m_{med} [GeV]	Γ/m_{med}	$\sigma \times A_{300}$ [fb]	$\sigma \times A_{500}$ [fb]
100	0.037	8.0e+01	7.0e+00
300	0.040	6.2e+01	6.5e+00
500	0.062	3.3e+01	4.0e+00

Figure 3.14: Scan over mediator mass. The $\not{E}_T$ distribution is compared for the scalar mediator models using the parameters as indicated. Ratios of the normalized distributions with respect to the first one are shown. A_{300} and A_{500} in the table denote the acceptance of the $\not{E}_T > 300\,\text{GeV}$ and $\not{E}_T > 500\,\text{GeV}$ cut, respectively.

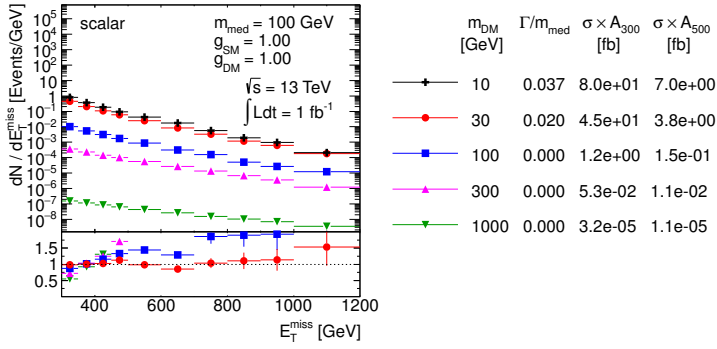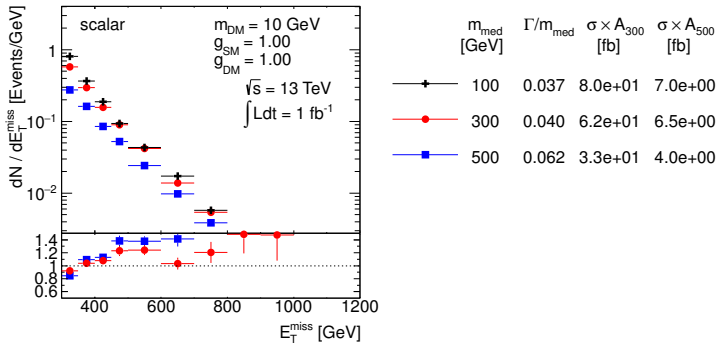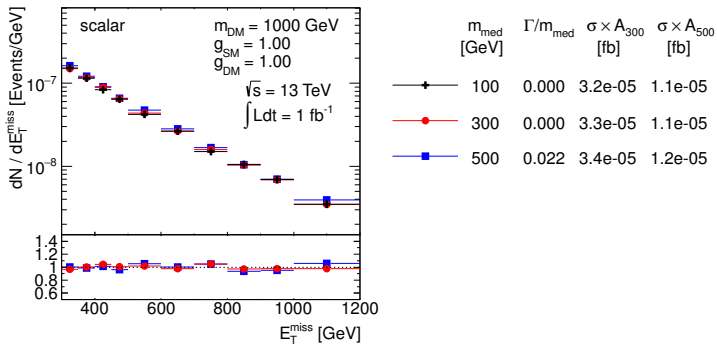| m_{med} [GeV]	Γ/m_{med}	$\sigma \times A_{300}$ [fb]	$\sigma \times A_{500}$ [fb]
100	0.000	3.2e-05	1.1e-05
300	0.000	3.3e-05	1.1e-05
500	0.022	3.4e-05	1.2e-05

Figure 3.15: Scan over mediator mass. The $\not{E}_T$ distribution is compared for the scalar mediator models using the parameters as indicated. Ratios of the normalized distributions with respect to the first one are shown. A_{300} and A_{500} in the table denote the acceptance of the $\not{E}_T > 300\,\text{GeV}$ and $\not{E}_T > 500\,\text{GeV}$ cut, respectively.

in the previous section. Therefore, a similar pattern is followed here, taking again $g_q = g_{DM} = 1$. Only the sensitivity to the highest mediator masses has to be revisited. The generator level cross section times the acceptance at $\not{E}_T > 500\,\text{GeV}$ for the model with couplings $g_q = g_{DM} = 1$, light Dark Matter of 10 GeV and 500 GeV scalar mediator is at the order of 10 fb, i.e. just at the edge of the early Run-2 sensitivity. Increasing the mediator mass to 1 TeV pushes the product $\sigma \times A$ down to approximately 0.1 fb, beyond the LHC sensitivity. Therefore, we choose to remove the 2 TeV mediator mass from the grid and present the final grid with 26 mass points only in Fig. 3.2. One point at very high mediator mass (5 TeV) is added for each of the DM masses scanned, to aid the reinterpretation of results in terms of contact interaction operators (EFTs).

m_{DM} (GeV)	m_{med} (GeV)								
1	10	20	50	100	200	300	500	1000	5000
10	10	15	50	100					5000
50	10		50	95	200	300			5000
150	10				200	295	500		5000
500	10						500	995	5000
1000	10							1000	5000

Table 3.2: Simplified model benchmarks for s−channel simplified models (spin-0 mediators decaying to Dirac DM fermions in the scalar and pseudoscalar case, taking the minimum width for $g_q = g_{DM} = 1$)

The proposal for the scan in the g_q–g_{DM} plane is described in the following section.

3.3 Cross section scaling

The aim of the parameter grid optimization is to find out whether certain parts of the parameter space can be omitted and one can rely on the neighboring grid points in order to populate the missing parts. There are two ways of doing this:

- Interpolation is used in-between the grid points that are close enough such that finer granularity is not needed for the presentation purposes, or between the points where smooth or no changes of the results are expected. The latter argument is exactly the one that motivates the reduction of the grid points in the M_{med}–m_{DM} plane.

- Recalculation of the results can be used when the dependencies with respect to the neighboring grid points are known.

The results of the scan over the couplings presented in the previous sections indicate there are no changes in kinematic distributions for different choices of the coupling strengths. This means that the

acceptance remains the same in the whole g_q–g_{DM} plane and it is
sufficient to perform the detector simulation only for one single grid
point. The resulting truth-level selection acceptance and the detector
reconstruction efficiency can then be applied to all remaining grid
points in the g_q–g_{DM} plane where only the generator-level cross sec-
tion needs to be known. This significantly reduces the computing
time as the detector response is by far the most expensive part of
the Monte Carlo sample production. However, a further step can be
taken if a parameterization of the cross section dependence from one
grid point to another exists, in which case the number of generated
samples can be reduced even further.

Let us now elaborate on a cross section scaling procedure. The
propagator on the s-channel exchange is written in a Breit-Wigner
form as $\frac{1}{\sqrt{s}-M_{med}^2+iM_{med}\Gamma}$. The relative size of the center-of-mass en-
ergy defined by the two partons entering the hard process and the
mediator mass allows to classify the production in the following way:

- off-shell production when $\sqrt{s} \gg M_{med}$ leading to suppressed cross
  sections,

- on-shell production when $\sqrt{s} \sim M_{med}$ leading to enhanced cross
  sections,

- effective field theory (EFT) limit when $\sqrt{s} \ll M_{med}$.

All three categories can be distinguished in Fig. 3.16 showing the up-
per limit on the interaction scale $M^* \equiv M_{med}/\sqrt{g_q g_{DM}}$ for vector
mediator. In the case of the off-shell production and the EFT limit,
the first term in the propagator dominates which reduces the de-
pendence on the mediator width. Therefore, in these cases one can
approximate the cross section as

$$\sigma \propto g_q^2 g_{DM}^2. \tag{3.15}$$

The on-shell production regime is the most interesting one as it gives
the best chances for a discovery at the LHC given the cross section
enhancement. The propagator term with the width cannot be ne-
glected in this case and, in the narrow width approximation, one can
integrate

$$\int \frac{ds}{(s - M_{med}^2)^2 + M_{med}^2\Gamma^2} = \frac{\pi}{M_{med}\Gamma} \tag{3.16}$$

which further implies the cross section scaling

$$\sigma \propto \frac{g_q^2 g_{DM}^2}{\Gamma}. \tag{3.17}$$

Since $\Gamma \sim g_q^2 + g_{DM}^2$, one can simplify this rule in the extreme cases as follows

$$\sigma \quad \propto \quad \frac{g_q^2 g_{DM}^2}{g_q^2 + g_{DM}^2} \xrightarrow{g_q \ll g_{DM}} g_q^2 \qquad (3.18)$$

$$\sigma \quad \propto \quad \frac{g_q^2 g_{DM}^2}{g_q^2 + g_{DM}^2} \xrightarrow{g_q \gg g_{DM}} g_{DM}^2 . \qquad (3.19)$$

However, it is important to keep in mind that there is no simple scaling rule for how the cross section changes with the Dark Matter mass, mediator mass and the mediator width because PDFs matter in such cases as well. Therefore, the scaling procedure outlined above is expected to work only for fixed masses and fixed mediator width.
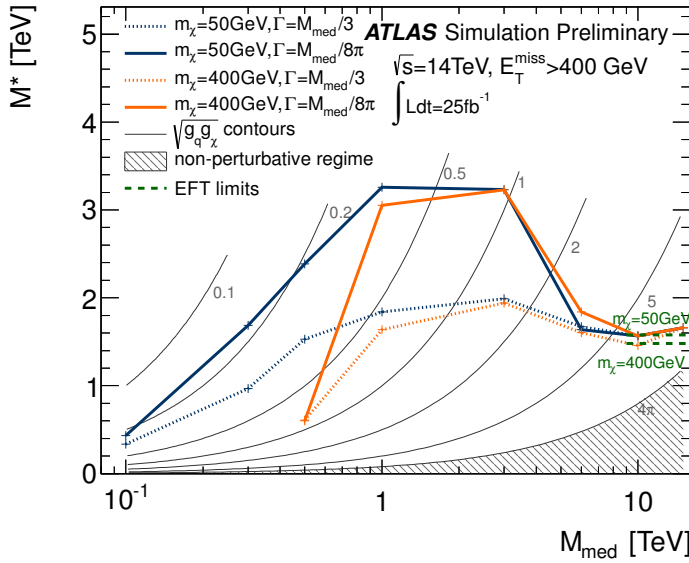

Figure 3.16: Comparison of the 95% CL lower limits on the scale of the interaction of a Z'-like simplified model at 14 TeV, in terms of the mediator mass. Corresponding limits from EFT models are shown on the same plot as green dashed lines to show equivalence between the two models for high mediator masses. Taken from Ref. [ATL14].

Figures 3.17 and 3.18 show the minimal width in the g_q–g_{DM} plane for all vector, axial-vector, scalar and pseudo-scalar mediators for $M_{med} = 100\,\text{GeV}$ and $1000\,\text{GeV}$, respectively, taking $m_{DM} = 10\,\text{GeV}$. The individual colors indicate the lines of constant width along which the cross section scaling works. For vector and axial-vector mediators, the minimal width is predominantly defined by g_q due to the number of quark flavors and the color factor. On the contrary, both the Standard Model and Dark Matter partial width have comparable contributions in case of scalar and pseudo-scalar mediators if the top quark channel is open ($M_{med} > 2m_t$). However, mostly g_{DM} defines the minimal width for $M_{med} < 2m_t$ due to the Yukawa-suppressed light quark couplings.

The performance of the cross section scaling is demonstrated in Fig. 3.19 where the mass point $M_{med} = 1\,\text{TeV}$ and $m_{DM} = 10\,\text{GeV}$

Figure 3.17: Minimal width for vector, axial-vector, scalar and pseudo-scalar mediators as a function of the individual couplings g_q and g_{DM}, assuming $M_{med} = 100\,\text{GeV}$ and $m_{DM} = 10\,\text{GeV}$.
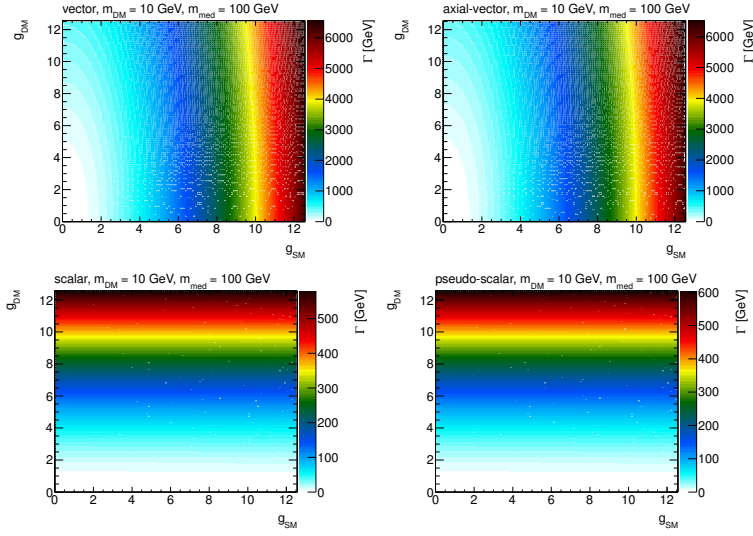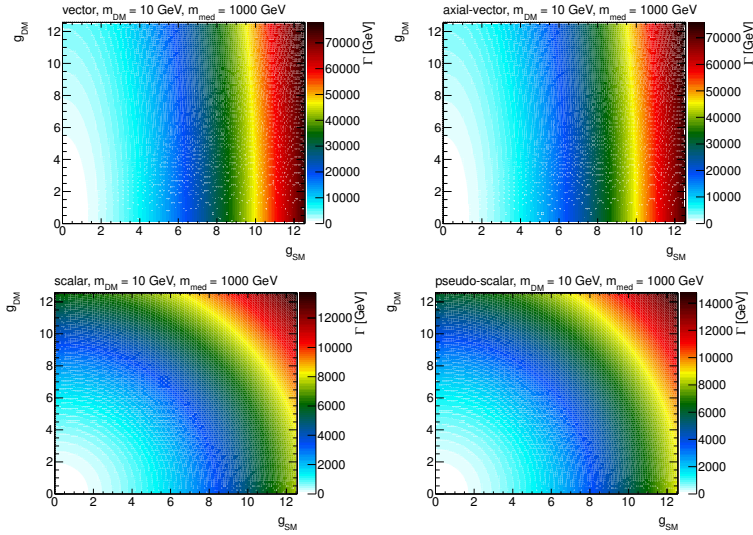

Figure 3.18: Minimal width for vector, axial-vector, scalar and pseudo-scalar mediators as a function of the individual couplings g_q and g_{DM}, assuming $M_{med} = 1\,\text{TeV}$ and $m_{DM} = 10\,\text{GeV}$.

is chosen and rescaled from the starting point $g_q = g_{DM} = 1$ according to Eq. 3.17 to populate the whole g_q–g_{DM} plane. This means the width is not kept constant in this test and this is done in purpose in order to point out deviations from the scaling when the width is altered. For each mass point, the rescaled cross section is compared to the generator cross section and the ratio of the two is plotted. For the given choice of the mass points, the scaling seems to work approximately with the precision of $\sim 20\%$ in the region where $\Gamma_{min} < M_{med}$. Constant colors indicate the lines along which the cross section scaling works precisely and there is a remarkable resemblance of the patterns shown in the plots of the mediator width. To prove the scaling along the lines of constant width works, one such line is chosen in Fig. 3.20 for a scalar mediator, defined by $M_{med} = 300\,\text{GeV}$, $m_{DM} = 100\,\text{GeV}$, $g_q = g_{DM} = 1$, and the rescaled and generated cross sections are found to agree within 3%.
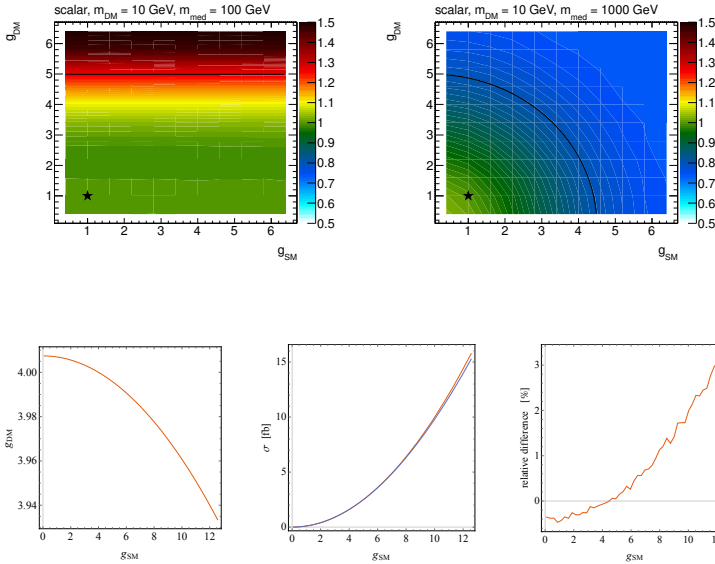
Figure 3.19: Ratio of the rescaled and generated cross sections in the g_q–g_{DM} plane. The point at $g_q = g_{DM} = 1$, taken as a reference for the rescaling, is denoted by a star symbol. Scalar model with $M_{med} = 100\,\text{GeV}$ (left) and 1 TeV (right) is plotted for $m_{DM} = 10\,\text{GeV}$. The limiting case $\Gamma_{min} = M_{med}$ is shown as a black line.

Figure 3.20: Scaling along the lines of constant width. The line of constant width for $M_{med} = 300\,\text{GeV}$ and $m_{DM} = 100\,\text{GeV}$, intercepting $g_q = g_{DM} = 4$ is shown on left. The generated and rescaled cross sections are compared in the middle, the corresponding ratio is shown on right.

Proposed parameter grid   We propose to present the results in the g_q–g_{DM} plane using the following prescription:

- Since the shapes of kinematic quantities do not change for different couplings, use the acceptance and efficiency for the available $m_{DM} = 50\,\text{GeV}$, $M_{med} = 300\,\text{GeV}$, $g_q = g_{DM} = 1$ grid point from the M_{med}–m_{DM} plane for the scalar and pseudo-scalar mediator. In case of the vector and axial-vector mediator, use the grid point $m_{DM} = 50\,\text{GeV}$, $M_{med} = 1\,\text{TeV}$, $g_q = g_{DM} = 1$.

- Generate additional samples in order to get generator cross sections only. For scalar and pseudo-scalar mediator, choose $m_{DM} =$

349   50 GeV, $M_{\text{med}} = 300$ GeV with the following values for $g_q = g_{\text{DM}}$:

350   0.1, 2, 3, 4, 5, 6. For vector and axial vector mediator, choose

351    $m_{\text{DM}} = 50$ GeV, $M_{\text{med}} = 1$ TeV with the following values for

352    $g_q = g_{\text{DM}}$: 0.1, 0.25, 0.5, 0.75, 1.25, 1.5. The upper values are de-

353   fined by the minimal width reaching the mediator mass.

354   • Rescale the generator cross sections along the lines of constant

355   width in order to populate the whole g_q–g_{DM} plane.

Rescaling to different mediator width   In general there may be an inter-
est to consider larger mediator masses than Γ_{min} in order to accom-
modate further couplings of the mediator. The cross section scaling
method described above can be used to reinterpret the results pre-
sented for the minimal width, since multiplying the width by factor n
is equivalent to changing the coupling strength by factor $\sqrt{n}$, i.e.

$$\sigma(g_q, g_{\text{DM}}, n\Gamma_{\text{min}}(g_q, g_{\text{DM}})) \propto \frac{g_q^2 g_{\text{DM}}^2}{\Gamma_{\text{min}}(\sqrt{n}g_q, \sqrt{n}g_{\text{DM}})} \ . \tag{3.20}$$

The cross section for the sample with couplings g_q and g_{DM} and
modified mediator width $\Gamma = n\Gamma_{\text{min}}$ can therefore be rescaled from
a sample generated with the minimal width corresponding to the
couplings scaled by $\sqrt{n}$ as described in the following formula.

$$\sigma(g_q, g_{\text{DM}}, n\Gamma_{\text{min}}(g_q, g_{\text{DM}})) = \frac{1}{n^2}\sigma(\sqrt{n}g_q, \sqrt{n}g_{\text{DM}}, \Gamma_{\text{min}}(\sqrt{n}g_q, \sqrt{n}g_{\text{DM}}))$$

$$\tag{3.21}$$

356   Advantage of doing this is again in the fact that no event selection

357   and detector response needs to be simulated since the changes in

358   couplings do not have an effect on the shapes of kinematic distribu-

359   tions.

360   ### 3.3.1   *POWHEG settings*

361   This section describes specific settings for the Dark Matter models

362   needed to run the POWHEG generation.

      • The POWHEG implementation allows to generate a single sample
        that provides sufficient statistics in all mono-jet analysis signal re-
        gions. POWHEG generates weighted events and the `bornsuppfact`
        parameter is used to set the event suppression factor according to

$$F(k_{\text{T}}) = \frac{k_{\text{T}}^2}{k_{\text{T}}^2 + \texttt{bornsuppfact}^2} \ . \tag{3.22}$$

363   In this way, the events at low $\not{E}_T$ are suppressed and receive higher

364   event weights which ensures higher statistics at high $\not{E}_T$. We rec-

365   ommend to set `bornsuppfact` to 1000.

- The `bornktmin` parameter allows to suppress the low $\not{E}_T$ region even further by starting the generation at a certain value of k_T. It is recommended to set this parameter to half the lower analysis $\not{E}_T$ cut, therefore the proposed value for `bornktmin` is 150.

- Set `runningwidth` to 0.

- Set `mass_low` and `mass_high` to -1.

- The minimal values for `ncall1`, `itmx1`, `ncall2`, `itmx2` are 250000, 5, 1000000, 5 for the DMV model, respectively. In order to increase speed, set `foldsci` and `foldy` to 2 and keep `foldphi` at 1.

- The minimal values for `ncall1`, `itmx1`, `ncall2`, `itmx2` are 100000, 5, 100000, 5 for the DMS_tloop model, respectively.

- Allow negative weights for the DMV model by setting `withnegweights` to 1.

- Since the DMS_tloop model is a leading order process, set `LOevents` and `bornonly` are set to 1 internally.

3.4 *Colored scalar mediator, t-channel exchange*

An alternative set of simplified models exist where the mediator is exchanged in the *t*-channel, thereby coupling the quark and dark matter particle directly. Under the assumption that χ is a Standard Model (SM) singlet, the mediating particle, labeled ϕ, is necessarily charged and coloured. This model is parallel to, and partially motivated by, the squark of the MSSM, but in this case the χ is chosen to be Dirac. Following the example of Ref. [PVZ14], the interaction Lagrangian is written as

$$\mathcal{L}_{\text{int}} = g \sum_{i=1,2,3} (\phi_L^i \bar{Q}_L^i + \phi_{uR}^i \bar{u}_R^i + \phi_{dR}^i \bar{d}_R^i)\chi \qquad (3.23)$$

(Note: [PVZ14] uses only i = 1,2, but I think it's fine to extend this to 3 here.) where Q_L^i, u_R^i and d_R^i are the SM quarks and ϕ_L^i, ϕ_{uR}^i and ϕ_{dR}^i are the corresponding mediators, which (unlike the *s*-channel mediators) must be heavier than χ. These mediators have SM gauge representations under $(SU(3), SU(2))_Y$ of $(3,2)_{-1/6}$, $(3,1)_{2/3}$ and $(3,1)_{-1/3}$ respectively. Variations of the model previously studied include coupling to the left-handed quarks only [CEHL14, BDSJ$^+$14], to the ϕ_{uR}^i [DNRT13] or ϕ_{dR}^i [PVZ14, A$^+$14b], or some combination [BB13, AWZ14].

Minimal Flavour Violation (MFV) requires that the mediator masses for each flavour be equal; the same logic also applies to the

couplings g. The available parameters are then

$$\{m_\chi, M_\phi, g\}. \tag{3.24}$$

In practice, the third mediator mass and coupling could be separated from the other two, if higher order corrections to the MFV prediction arise due to the large top Yukawa coupling – a common variation is then to define this split between the first two generations and the third, so the parameters are extended to

$$\{m_\chi, M_{\phi_{1,2}}, M_{\phi_3}, g_{1,2}, g_3\}. \tag{3.25}$$

The width of each mediator is expressed, using the example of decay to an up quark, as

$$\Gamma(\phi_i \to \bar{u}_i \chi) = \frac{g_i^2}{16\pi M_{\phi_i}^3} (M_{\phi_i}^2 - m_{u_i}^2 - m_\chi^2)$$
$$\times \sqrt{M_{\phi_i}^4 + m_{u_i}^4 + m_\chi^4 - 2M_{\phi_i}^2 m_{u_i}^2 - 2M_{\phi_i}^2 m_\chi^2 - 2m_{u_i}^2 m_\chi^2}, \tag{3.26}$$

this reduces to

$$\frac{g_i^2 M_{\phi_i}}{16\pi} \left(1 - \frac{m_\chi^2}{M_{\phi_i}^2}\right)^2 \tag{3.27}$$

in the limit $M_{\phi_i}, m_\chi \gg m_{u_i}$.

An interesting point of difference with the s-channel simplified models is that the mediator can radiate a SM object, such as a jet or gauge boson, thus providing three separate mono-X diagrams which must be considered together in calculations. This model can also give a signal in the di-jet + MET channel when, for example, the χ is exchanged in the t-channel and the resulting ϕ pair each decay to a jet + χ.

4

Specific models for signatures with EW bosons

In this Section, we consider models with a photon, a W boson, a
Z boson or a Higgs boson in the final state, accompanied by Dark
Matter particles that either couple directly to the boson or are medi-
ated by a new particle. The experimental signature is identified as
V+MET.

These models are interesting both as extensions of models where
the gluon provides the experimentally detectable signature, and as
stand-alone models with final states that cannot be generated by the
models in Section 3.
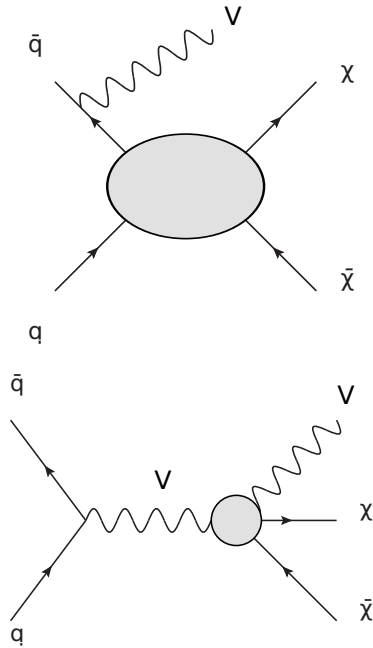

Figure 4.1: Sketch of benchmark
models including a contact interac-
tion for V+MET searches, adapted
from [NCC+14].

The models considered can be divided in three categories:

Models including a contact operator, where the boson is radiated from the initial state
As depicted in the top diagram of Figure 4.1, these models follow
the nomenclature and theory for the EFT benchmarks commonly

used by MET+X searches [GIR$^+$10]. These models have been used in past experimental searches [Kha14, Aad14b, K$^+$14, Aad14b, A$^+$14a, Aad14a], and they will not be described here.

Models including a contact operator, where the boson is directly coupled to DM Shown in the bottom of Figure 4.1, these models allow for a contact interaction vertex that directly couples the boson to Dark Matter.

Simplified models where the boson is radiated from the initial state These models follow those already described in Section 3, replacing the initial state gluon with a boson.

V-specific simplified models These models postulate direct couplings of new mediators to bosons, e.g. they couple the Higgs boson to a new scalar [CDM$^+$14].

The following Sections describe the models within these categories, the parameters for each of the benchmark models chosen, the studies towards the choices of the parameters to be scanned, and finally point to the location of their Matrix Element implementation.

4.1 *Simplified models with ISR boson radiation*

Searches in the jet+MET final state are generally more sensitive with respect to final states including bosons, due to the much larger rates of signal events featuring quark or gluon radiation with respect to radiation of bosons [ZBW13], in combination with the low branching ratios if leptons from boson decays are required in the final state. The rates for the Higgs boson radiation is too low for these models to be considered a viable benchmark [CDM$^+$14]. However, the presence of photons leptons from W and Z decays and W or Z bosons decaying hadronically allows to reject the background more effectively, making Z/gamma/W+MET searches still worth comparing with searches in the jet+MET final state.

4.1.1 *Vector mediator exchanged in the s-channel*

The case for searches with W bosons in the final state has so far been strenghtened by the presence of particular choices of couplings between the WIMP and the up and down quarks which enhance W radiation [BT13], in the case of the exchange of a vector mediator in the s-channel. Run-1 searches have considered three sample cases for the product of up and down quark couplings to the mediator ξ:

- No couplings between mediator and either up or down quarks ($\xi = 0$);

- Same coupling between mediator and each of the quark types ($\xi = 1$);

- Coupling of opposite sign between mediator and each of the quark types ($\xi = -1$).

The $\xi = -1$ case leads to a large increase in the cross-section of the process, and modifies the spectrum of missing transverse energy or transverse mass used for the searches. The sensitivity of the W+MET search for this benchmark in this case surpasses that of the jet+MET search. However, as shown in Ref. [BCD+15], the cross-section increase is due to the production of longitudinally polarized W bosons, as a consequence of a violation of electroweak gauge symmetries. Unless further particles are introduced (in a fashion similar to the Higgs boson in the Standard Model), choosing a value of $\xi = -1$ for this simplified model will lead to a manifest violation of unitarity at LHC energies. The simplified model with a vector mediator exchanged in the s-channel model can still be considered as a benchmark for searches with a W boson if $\xi = 1$. We leave the study of further models with cross-section enhancements due to different couplings to up and down quarks for studies beyond the early LHC searches covered in this document. An example of such model is the case of both DM and SM Higgs charged under a new U(1)′, with a a small mass mixing between SM Z-boson and the new Zprime. This leads to different effective DM couplings to u_L and d_L, proportional to their coupling to the Z boson, detailed in Appendix B.

The scan in the parameters that characterize this simplified model for EW boson + MET searches follow what already detailed in Section 3.

As in the case of the jet+MET models, the width does not have a significant impact on the kinematic distributions relevant for those searches. An example of the particle-level analysis acceptance using the generator-level cuts from Ref. [Aad15] for the photon+MET analysis, but raising the photon p_T cut to 150 GeV is shown in Figure 4.2, comparing a width that is set to $\Gamma = M_{med}/3$ to the minimal width (the ratio between the two widths ranges from 1.05 to 1.5 with increasing mediator masses).

Examples of relevant kinematic distributions for selected benchmark points are shown in Fig. 4.9; leading-order cross-sections for the chosen benchmark points are shown in Table **?? [TODO: Insert table of cross-sections]**.

4.1.2 *Colored scalar mediator exchanged in the t-channel*

The model parameters with emission of an EW boson follow those in Section 3.
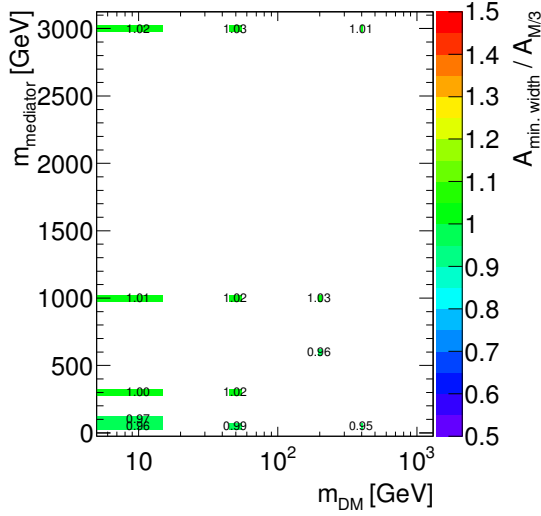
Figure 4.2: Analysis acceptance for the photon+MET analysis when varying the mediator width, in the case of a vector mediator exchanged in the $s-$channel

Figure 4.4 shows the MET distribution for the hadronic Z+MET final state, with varying dark matter and mediator mass, before any selection. The acceptance for a series of simplified analysis cuts (MET>350 GeV, leading jet $p_T > 40$ GeV, minimum azimuthal angle between jet and MET > 0.4) applied at the generator level is shown in Figure 4.5.

The parameter scan is still under discussion.

4.1.3 *Model implementation*

These models are generated at leading order with MadGraph 2.2.2, and parameter cards can be found on SVN **[TODO: Add SVN location]**. The parton shower is done using Pythia 8, with a matching scale of... **[TODO: To be completed.]**

4.2 *EFT models with direct DM-boson couplings*

[Linda Carpenter and Uli Haisch are rewriting this section. Changes expected:

- **change of normalization and Lagrangians to be consistent with [CHH15], linked to notation of [CNS$^+$13]**

- **description of dimension-5 EFTs**

- **addition of a dimension-5 simplified model]**

A complete list of effective operators with direct DM/boson couplings for Dirac DM, up to dimension 7, can be found in [CHLR13].
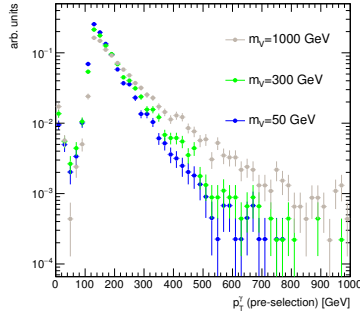
Figure 4.3: Kinematic distributions relevant for searches with W, Z and photons in the final state, for the simplified model with a vector mediator exchanged in the s−channel.

(a) Missing transverse momentum distribution for the photon+MET final state, for different mediator mass choices, for a DM mass of 10 GeV.
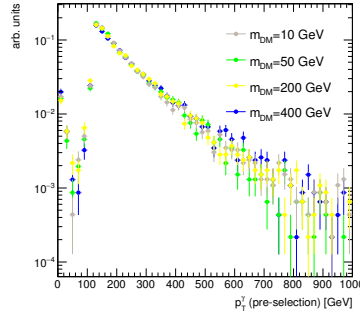
(b) Leading photon transverse momentum distribution for the photon+MET final state, for different DM mass choices, with a mediator mass of 1 TeV.
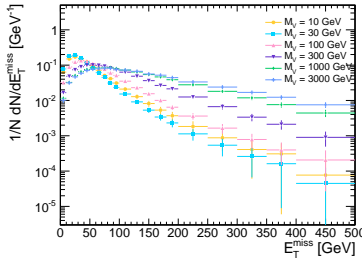
(c) Missing transverse momentum distribution for the leptonic Z+MET final state, for different mediator mass choices, for a DM mass of 15 GeV

(d) Transverse mass (m_T) for the leptonic W+MET final state.

(e) Missing transverse momentum distribution for the hadronic W+MET final state.

Following the notation of [CNS+13], the dimension 5 benchmark models from this category have a Lagrangian that includes terms
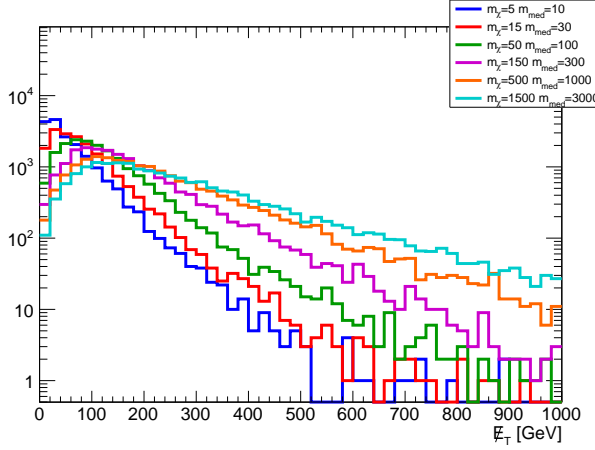
Figure 4.4: Missing transverse momentum distribution for the hadronic Z+MET final state, for the simplified model with a colored scalar mediator exchanged in the $t-$channel.
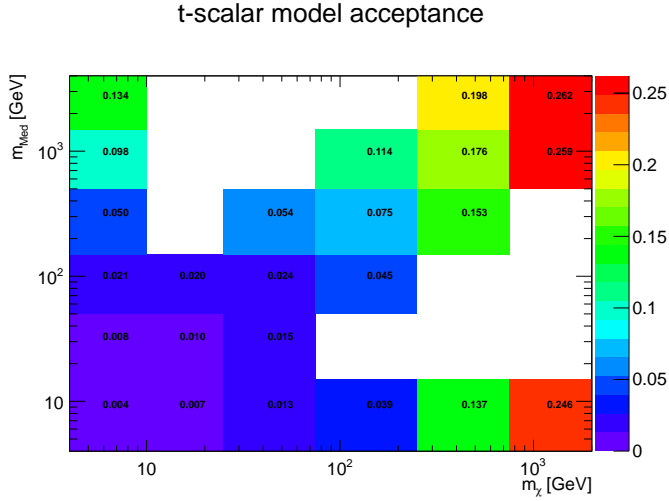
Figure 4.5: Acceptance table for the hadronic Z+MET final state, for the simplified model with a colored scalar mediator exchanged in the $t-$channel.

such as:

$$\frac{m_W^2}{\Lambda_5^3} \, \bar{\chi}\chi \, W^{+\mu}W_\mu^- + \frac{m_Z^2}{2\Lambda_5^3} \, \bar{\chi}\chi \, Z^\mu Z_\mu \, . \tag{4.1}$$

where m_Z and m_W are the masses of the Z and W boson, W^μ and Z^μ are the fields of the gauge bosons, χ denote the Dark Matter fields and Λ_5 is the effective field theory scale. This operator induces signatures with MET in conjunction with Z and W bosons at tree level, while at loop level it induces couplings to photon pairs and $Z\gamma$ through W loops. **[TODO: Ask Linda to explain this better than I did.]**. In these models, a clear relation exists between final states with photons, EW bosons and Higgs boson. **[TODO: see if mono-Higgs**

545 **studies exist for these operators, include them here]**.

546   The dimension 7 benchmark models include couplings to the

547 kinetic terms of the EW bosons ($F_i^{\mu\nu}$, with $F_i = 1, 2, 3$ being the field

548 strengths of the SM $U(1)$ and $SU(2)$ gauge groups and $\tilde{F}_i^{\mu\nu}$ their dual

549 tensors). The Lagrangian for the scalar coupling of DM and bosons

550 include terms such as the following:

$$\frac{1}{\Lambda_{7,S}^3} \, \bar{\chi}\chi \, \sum_i k_i F_i^{\mu\nu} F_{\mu\nu}^i + \frac{1}{\Lambda_{7,S}^3} \, \bar{\chi}\chi \, \sum_i k_i F_i^{\mu\nu} \tilde{F}_{\mu\nu}^i \tag{4.2}$$

551   The Lagrangian with pseudoscalar coupling includes the following

552 terms:

$$\frac{1}{\Lambda_{7,PS}^3} \, \bar{\chi}\gamma^5\chi \, \sum_i k_i F_i^{\mu\nu} F_{\mu\nu}^i + \frac{1}{\Lambda_{7,PS}^3} \, \bar{\chi}\gamma^5\chi \, \sum_i k_i F_i^{\mu\nu} \tilde{F}_{\mu\nu}^i \tag{4.3}$$

553   The cut-off scales Λ for the separate terms can be related to op-

554 erators with different Lorentz structure from Ref. [CHLR13]. Given

555 that they do not lead to substantial differences for collider searches as

556 shown in Figure 2 of Ref. [CNS+13], they have been denoted as $\Lambda_{7,S}$

557 for the scalar case and $\Lambda_{7,PS}$ for the pseudoscalar case.

558   The k_i coefficients for the dimension 7 models are related to the

559 couplings of DM to pairs of gauge bosons by gauge invariance:

$$g_{WW} \;=\; \frac{2k_2}{s_w^2 \Lambda_7^3} \tag{4.4}$$

$$g_{ZZ} \;=\; \frac{1}{4s_w^2 \Lambda_7^3} \left(\frac{k_1 s_w^2}{c_w^2} + \frac{k_2 c_w^2}{s_w^2} \right) \tag{4.5}$$

$$g_{\gamma\gamma} \;=\; \frac{1}{4c_w^2} \frac{k_1 + k_2}{\Lambda_7^3} \tag{4.6}$$

$$g_{Z\gamma} \;=\; \frac{1}{2s_w c_w \Lambda_7^3} \left(\frac{k_2}{s_w^2} - \frac{k_1}{c_w^2} \right) \tag{4.7}$$

560   where s_w and c_w are respectively the sine and cosine of the weak

561 mixing angle.

562   The coefficients k_i determine the relative importance of each of

563 the boson channels, and their correlations. For example, for what

564 concerns searches with W, Z and photons:

565 • k_2 alone controls the rate of the coupling to W boson pairs;

566 • If $k_1 = k_2$ contributions from both Z and γ exchange appear;

567 • If $k_1 = c_w^2/s_w^2 k_2$ the γ exchange is negligible.

568   The coefficients k_1 and k_2 are related to the coefficients c_1 and

569 c_2 in the equivalent models of Ref. [CHH15] as $k_2 = s_w^2 * c_2$ and

570 $k_1 = c_w^2 * c_1$.

571 **[TODO: Linda will possibly complete/correct this subsection]**
572 UV completions of such operators where the dominant signature
573 is a single photon or EW boson are possible, for example through
574 the exchange of a W′ or a Z′. They are left as benchmarks for future
575 searches as their implementation may require loop diagrams and
576 need further studies beyond the timescale of this Forum.
577   As shown in Fig. 4.6 kinematics of this model can be approxi-
578 mated by that of a simplified model including a high-mass scalar
579 mediator exchanged in the s-channel. For this reason, the list of
580 benchmark models with direct boson-DM couplings only includes
581 dimension 7 operators.
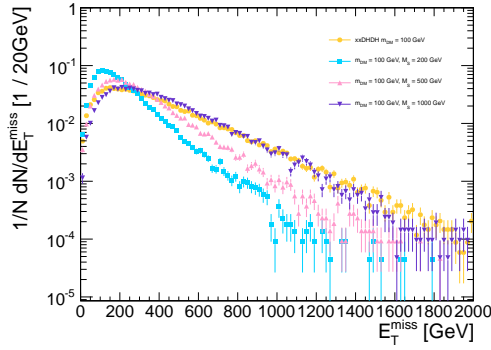
Figure 4.6: Comparison of the missing transverse momentum for the simplified model where a scalar mediator is exchanged in the s-channel and the model including a dimension-5 scalar contact operator, in the leptonic Z+MET final state

582   The kinematic distributions for dimension-7 scalar and pseu-
583 doscalar operators only shows small differences, as shown in Fig. 4.7.

Figure 4.7: Comparison of the missing transverse momentum for the scalar and pseudoscalar operators with direct interaction between DM and photon, in the photon+MET final state

584   Similarly, the differences in kinematics for the various signatures
585 are negligible when changing the coefficients k_1 and k_2, as shown in
586 Figure **??**. Only the case $k_1 = k_2 = 1$ is generated as benchmark; other
587 cases are left for reinterpretation as they will only need a rescaling of
588 the cross-sections shown in Table **?? [TODO: add tables with cross**
589 **sections]** for the various Dark Matter mass points considered.
590   Examples of relevant kinematic distributions for selected bench-
591 mark points are shown in Fig. 4.9.

(a) Missing transverse momentum distribution for the photon+MET final state.

Figure 4.8: Kinematic distributions relevant for searches with W, Z and photons in the final state, for for the scalar and pseudoscalar operators representing direct interactions between DM and bosons.

(b) Missing transverse momentum distribution for the leptonic Z+MET final state.

(c) Transverse mass (m_T) for the leptonic W+MET final state.

4.2.1 *Specific simplified models*

Mono-Higgs, to be completed...

(a) Missing transverse momentum distribution for the photon+MET final state.

(b) Missing transverse momentum distribution for the leptonic Z+MET final state.

(c) Transverse mass (m_T) for the leptonic W+MET final state.

(d) Fat **[Insert algorithm]** jet mass (m_T) for the the hadronic W+MET final state.

Figure 4.9: Kinematic distributions relevant for searches with W, Z and photons in the final state, for the simplified model with a vector mediator exchanged in the $s-$channel.

5

Specific models for signatures with heavy flavor quarks

5.1 $b\bar{b}$+MET models

5.2 Models with a single $b-$quark + MET

5.3 $t\bar{t}$+MET models

As described in Section 3.2, a model with a scalar/pseudoscalar particle mediating the DM-SM interactions is one of the simplest UV completions of our EFT models.

The expected signal of DM pair production depends on the production rate defined by the dark matter mass m_χ, mediator $m_{\phi/a}$, on the couplings g_i and on the branching ratio defined by the total decay width of the mediator ϕ/a. We calculate the minimum possible width (assuming only decays into the dark matter and the Standard Model fermions) that is consistent with a given value of $g_\chi g_q$, and assuming all couplings to SM particles equal $g_q = g_u = g_d = g_\ell$. These are given by Eq. (5.1) [BFG15].

$$\Gamma_{\phi,a} = \sum_f N_c \frac{y_f^2 g_q^2 m_{\phi,a}}{16\pi} \left(1 - \frac{4m_f^2}{m_{\phi,a}^2}\right)^{3/2} + \frac{g_\chi^2 m_{\phi,a}}{8\pi} \left(1 - \frac{4m_\chi^2}{m_{\phi,a}^2}\right)^{3/2}$$
$$+ \frac{\alpha_s^2 y_t^2 g_q^2 m_{\phi,a}^3}{32\pi^3 v^2} \left|f_{\phi,a}\left(\frac{4m_t^2}{m_{\phi,a}^2}\right)\right|^2 \tag{5.1}$$

where

$$f_\phi(\tau) = \tau\left[1 + (1-\tau)\arctan^2\left(\frac{1}{\sqrt{\tau-1}}\right)\right], \qquad f_a(\tau) = \tau\arctan^2\left(\frac{1}{\sqrt{\tau-1}}\right). \tag{5.2}$$

The first term in each width corresponds to the decay into SM fermions, and the sum runs over all kinematically available fermions, $N_c = 3$ for quarks and $N_c = 1$ for leptons. The second term is the decay into DM, assuming that is kinematically allowed. The factor

of two between the decay into SM fermions and into DM is a result of our choice of normalization of the Yukawa couplings due to spin dependencies. The last two terms correspond to decay into gluons. Since we have assumed that $g_q = g_u = g_d = g_\ell$, we have included in the partial decay widths $\Gamma(\phi/a \to gg)$ only the contributions stemming from top loops, which provide the by far largest corrections given that $y_t \gg y_b$ etc. At the loop level the mediators can decay not only to gluons but also to pairs of photons and other final states if kinematical accessible. However the decay rates $\Gamma(\phi/a \to gg)$ are always larger than the other loop-induced partial widths, and in consequence the total decay widths $\Gamma_{\phi/a}$ are well approximated by the corresponding sum of the individual partial decay widths involving DM, fermion or gluon pairs. It should be noted that if $m_{\phi/a} > 2m_t$ the total widths of ϕ/a will typically be dominated by the partial widths to top quarks.

5.3.1   *Parameter scan*

As discussed in Sec. 3.2, the MFV assumption for spin-0 mediators leads to quark mass dependent Yukawa couplings, and therefore dominant couplings to top quarks. This motivates dedicated DM+$t\bar{t}$ searches. The benchmark chosen for these searches follows the assumptions mentioned in the previous Section: we consider a Dirac fermion DM particle, universal couplings to quarks, and minimum mediator width.

The benchmark points scanning the model parameters have been selected to ensure that the kinematic features of the parameter space are sufficiently represented. Detailed studies were performed to identify points in the m_{DM}, $m_{\phi,a}$, g_{DM}, g_q (and $\Gamma_{\phi,a}$) parameter space that differ significantly from each other in terms of expected detector acceptance. Because missing transverse momentum is the key observable for searches, the mediator p_T spectra is taken to represent the main kinematics of a model. Another consideration in determining the set of benchmarks is to focus on the phase space where we expect the searches to be sensitive during the 2015 LHC run. Based on a projected integrated luminosity of $30\,\mathrm{fb}^{-1}$ expected for 2015, we disregard model points with a cross section times branching ratio smaller than 0.1 fb.

5.3.2   *Parameter scan*

The kinematics is most dependent on the masses m_{DM} and $m_{\phi,a}$. Figure 5.1 and 5.2 show typical dependencies for scalar and pseudoscalar couplings respectively. Typically, the mediator p_T spectra broadens with larger $m_{\phi,a}$. The kinematics are also quite different

656 between on-shell and off-shell production. Furthermore, the kine-
657 matic differences between scalar and pseudoscalar are large with
658 light mediator masses and are reduced for larger masses. It is there-
659 fore important to benchmark points covering on-shell and off-shell
660 production with sufficient granularity.
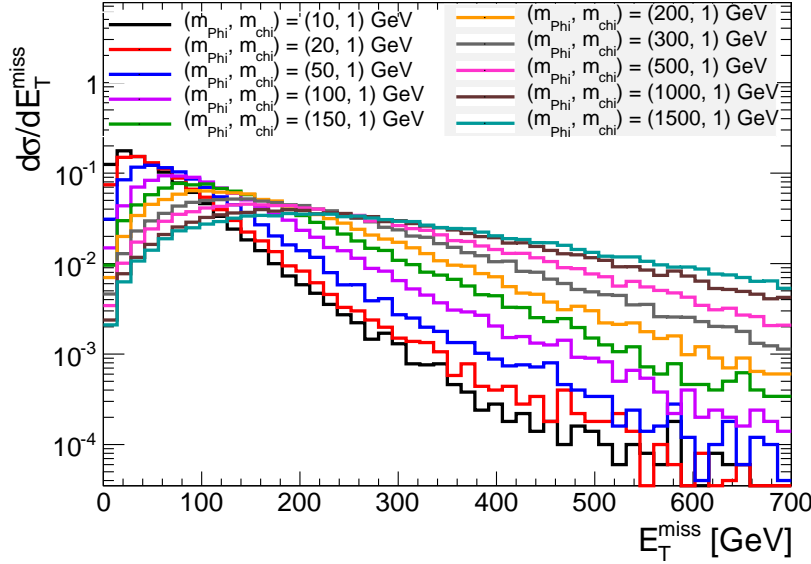
Figure 5.1: Example of the dependence of the kinematics on the scalar mediator mass. The Dark Matter mass is fixed to be 1GeV.

661 Typically only weak dependencies on width or equivalently cou-
662 plings are observed (see Fig 5.4), except for large mediator masses
663 of $\sim 1.5\,\text{TeV}$ or for very small couplings of $\sim 10^{-2}$. These regimes
664 where width effects are significant have production cross sections
665 that are too small to be relevant for $30\,\text{fb}^{-1}$ and are not considered
666 here. However, with the full Run-2 dataset, such models may be
667 within reach. The weak dependence on the typical width values can
668 be understood as the parton distribution function are the dominant
669 effect on mediator production. In other words, for couplings $\sim O(1)$
670 the width is large enough that the p_T of the mediator is determined
671 mainly by the PDF.
672 Another case where the width can impact the kinematics is when
673 $m_{\phi,a}$ is slightly larger than $2m_\chi$. Here, the width determines the rel-
674 ative contribution between on-shell and off-shell production. An
675 example is given in Fig. 5.5. In our recommendations we propose to
676 use for simplicity the minimal width, as this is represents the most
677 conservative choice to interpret the LHC results. **[TODO: mention
678 larger widths too]**
679 Given that the kinematics are similar for all couplings $\sim O(1)$,
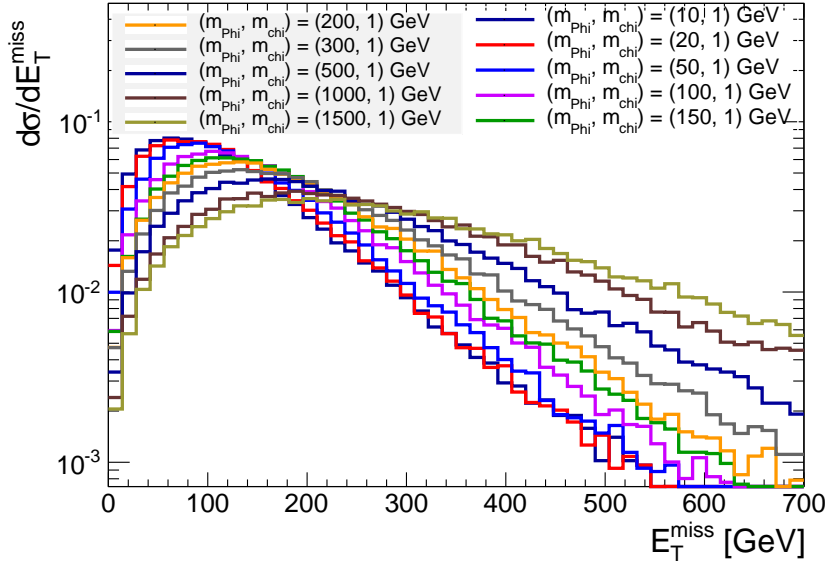
Figure 5.2: Example of the dependence of the kinematics on the pseudoscalar mediator mass. The Dark Matter mass is fixed to be 1GeV.
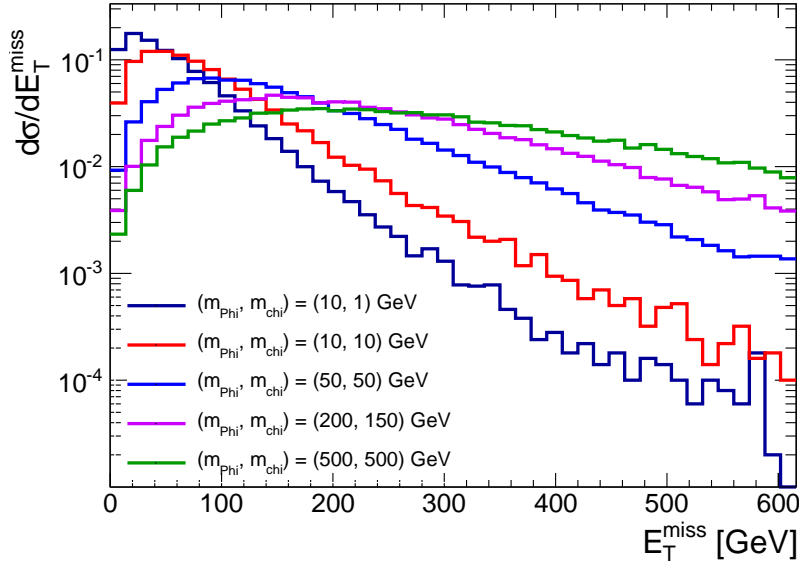
Figure 5.3: Example of the dependence of the kinematic for points of the grid proposed in Tab. 3.2 close to the $m_{\phi,a} \sim 2m_\chi$ limit.3

we recommend to generate only samples with $g_{DM} = g_q = 1$. It follows from this that these benchmark points should be a good approximation for non-unity couplings and for $g_{DM} \neq g_q$, provided that the sample is rescaled to the appropriate cross section times
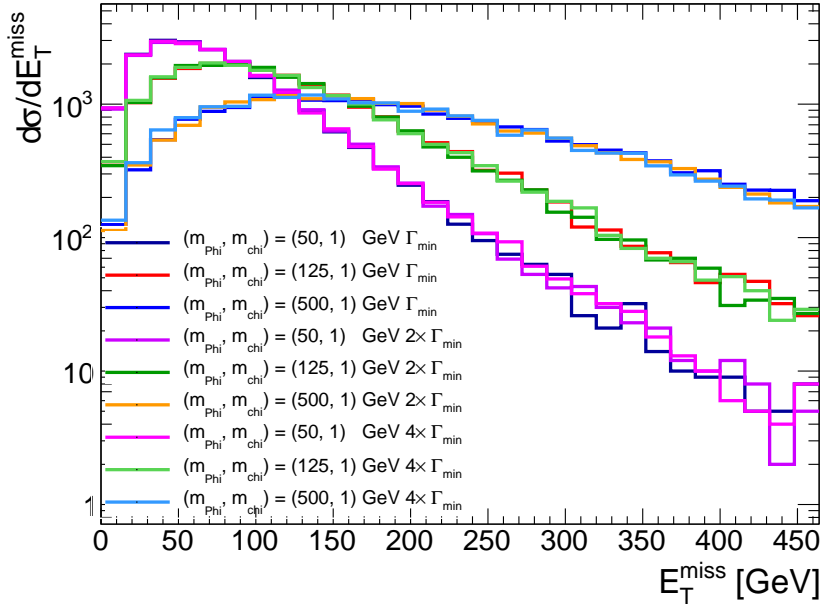
Figure 5.4: Study of the dependence of kinematics on the width of a scalar mediator. The width is increased up to four times the minimal width for each mediator and dark matter mass combination.
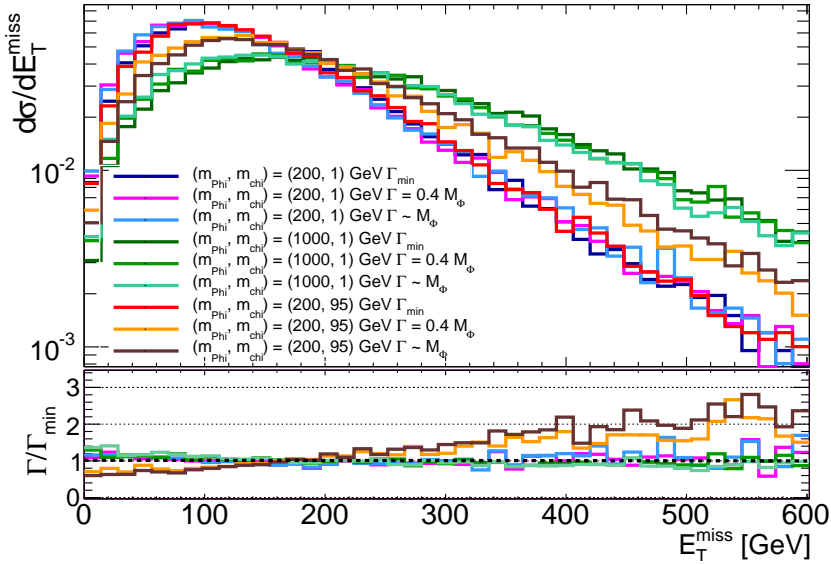
Figure 5.5: Dependence of the kinematics on the width of a scalar mediator. The width is increased up to the mediator mass. Choices of mediator and dark matter masses such that $m_{\phi,a}$ is slightly larger than $2m_\chi$ is the only case that shows a sizeable variation of the kinematics as a function of the width.

branching ratio. While the simple scaling function $\sigma' * BR' = [\sigma * BR] * (g'_q/g_q)^2 * (g'_{DM}/g_{DM})^2 * (\Gamma/\Gamma')$ is sufficient for a limited range of coupling values (see Fig. 5.6 for example), we also choose to

687   provide instead a table of cross section times branching ratio values
688   over a large range of couplings to support interpretation of search
689   results (see the Appendix C). The table lists couplings from $g = 0.1$ to
690    $g = 3.5$, where the upper limit is chosen to close to the perturbative
691   limit.
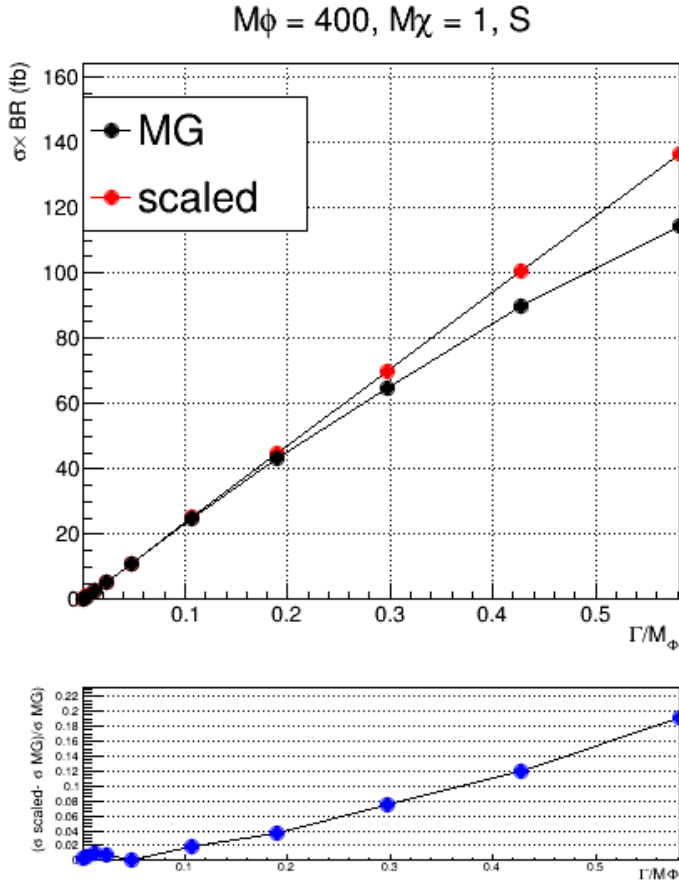
Figure 5.6: An example comparing a simple cross section scaling versus the computation from the generator, for a scalar model with $m_\phi = 400$ GeV, $m_{DM} = 1$ GeV and all couplings set to unity. In this example, the scaling relationship holds for Γ_ϕ/m_ϕ below 0.2, beyond which finite width effects become important and the simple scaling breaks down.

692   The points for the parameter scan chosen for this model are listed
693   in Table 3.2, chosen to be harmonized with those for other analyses
694   employing the same scalar model as benchmark. Based on the sensi-
695   tivity considerations above, DM masses are only simulated up to 500
696   GeV, leading to a total of 24 benchmark points.
697   In addition to the considerations discussed in the preceding sub-
698   sections, very light DM fermions are included ($m_{DM} = 10$ GeV) as
699   this is a region where colliders have a complementary sensitivity to

current direct detection experiments.

5.4 *Models with a single top−quark + MET*

Many different theories predict final states with a single top and as-
sociated missing transverse momentum (monotop), some of them
including dark matter candidates. A simplified model encompass-
ing the processes leading to this phenomenology is described in
Refs. [AFM11, AAB$^+$14, BCDF15], and is adopted as one of the
benchmarks for Run 2 LHC searches.

A dark matter candidate χ and a new particle M (vector or scalar)
are added to the SM, in a theory that respects the $\text{SU}(2)_L \times \text{U}(1)_Y$
symmetry and produces a single top quark in association with either
the DM particle or a new particle decaying invisibly.

Within this model, two distinct processes can lead to monotop
production:

* resonant production, as shown in the diagram of Fig. 5.7 (a),
  where a scalar (S in the figure, φ in the following) or vector (X)
  field are exchanged in the s-channel, and decay into the a spin 1/2
  invisible DM candidate (called f_{met} in the figure) and a top quark;

* non-resonant production, as shown in the diagrams of Fig. 5.7 (b)
  and (c), where a flavor-changing interaction produces a top quark
  in association with a new colored scalar (Φ) or vector (V). The new
  colored particles, called v_{met} in the figure, decay invisibly, e.g. to a
  pair of DM particles. v_{met} can also decay into a top quark and an
  up quark, leading to a same-sign top quark final state; a detailed
  study of the complementarity of this signature is beyond the scope
  of this Forum report.

In the following, resonant and non-resonant production are treated
independently as separate benchmarks. Only the case of a scalar
resonance is considered for the resonant model, while the case of
vector resonances is left for future studies.

Resonant production

In this case, a colored 2/3-charged scalar ($\varphi^{\pm}$) is produced reso-
nantly and decays into a top quark and a spin-1/2 invisible particle,
χ. The dynamics of the new sector is described by the following La-
grangian:

$$
\begin{aligned}
\mathcal{L} = \Big[& \varphi \bar{d}^c \big[a^q_{SR} + b^q_{SR}\gamma_5 \big] d + \varphi \bar{u} \big[a^{1/2}_{SR} + b^{1/2}_{SR}\gamma_5 \big] \chi \\
& + X_\mu \bar{d}^c \gamma^\mu \big[a^q_{VR} + b^q_{VR}\gamma_5 \big] d + X_\mu \bar{u} \gamma^\mu \big[a^{1/2}_{VR} + b^{1/2}_{VR}\gamma_5 \big] \chi + \text{h.c.} \Big] .
\end{aligned}
\tag{5.3}
$$

(a)

(b)   (c)

where u (d) stands for any up-quark ($down$-quark), the index S (V) stands for scalar (vector) field, and the index q runs over the three quark generations.

In the notation of [AAB$^+$14], the couplings of the new colored fields to down-type quarks are embedded into the 3×3 matrices $a^q_{\{S,V\}R}$ (scalar/vector couplings) and $b^q_{\{S,V\}R}$ (pseudoscalar/axial vector couplings) while those to the DM candidate χ and one single up-type quarks are given by the three-component vectors $a^{1/2}_{\{S,V\}R}$ and $b^{1/2}_{\{S,V\}R}$ in flavor space.

In the following, we only consider the model with a new colored scalar, as the requirement of invariance under $SU(2)_L X U(1)_Y$ would require the introduction of further particles in the case of a new colored vector [BCDF15].

Non-Resonant production

For the non-resonant production, the top quark is produced in association with the new particle: either a new scalar (ϕ) or a new vector (V). For simplicity, we only consider the case of a vector new particle, as the scalar case would involve a mixing with the SM Higgs boson and therefore a larger parameter space. The Lagrangian describing the dynamics of the non-resonant case is:

$$\mathcal{L} = \left[\phi \bar{u} \left[a^0_{FC} + b^0_{FC} \gamma_5 \right] u + V_\mu \bar{u} \gamma^\mu \left[a^1_{FC} + b^1_{FC} \gamma_5 \right] u + \text{h.c.} \right] . \quad (5.4)$$

The strength of the interactions among these two states and a pair of up-type quarks is modeled via two 3×3 matrices in flavor

space $a_{FC}^{\{0,1\}}$ for the scalar/vector couplings and $b_{FC}^{\{0,1\}}$ for the pseu-
doscalar/axial vector couplings.

Model parameters and assumptions

The models considered as benchmarks for the first LHC searches
contain further assumptions in terms of the flavour and chiral struc-
ture of the model with respect to the full Lagrangians of equa-
tions (5.3) and (5.4). These assumptions are qualitatively discussed
below.

Assumptions in the flavour and chiral structure of the models   We only
consider right-handed quark components, in order to simplify the
model phenomenology. The representation of the left-handed com-
ponents under the $SU(2)_L$ symmetry would lead to a coupling to
down-type quarks, since the effective theory is invariant under
$SU(2)_L \times U(1)_Y$ gauge symmetry. Having a coupling between the
new particle and *down*-type quarks would complicate the collider
phenomenology, adding the $V \rightarrow b\bar{d} + \bar{b}d$ decay mode in addition
to the invisible decay mode. This in turn sets the scalar (vector) and
pseudoscalar (axial vector) matrices to have elements of equal values.
Furthermore, in order to be visible at the LHC in the monotop
final state, these models must include a strong coupling between
the new particle ϕ and $t\chi$. The same kind of assumption exists for
the non-resonant production. This means that only the couplings
between the new scalar resonance and light quarks (a_{VR}, a_{SR}), and
the couplings between the new vector, the top quark and light quarks
(a_{FC}), are set to non-zero values

$$(a_{VR}^q)_{11} = (a_{VR}^{1/2})_3 = a \tag{5.5}$$

Implementation

This Section describes the notations used in the MadGraph model
convention, in term of the ones introduced in the previous Section.

The Madgraph model [Fuk] used for these benchmarks corre-
sponds to the Lagrangian from [AFM11]. Each coupling constant
of this dynamics can be set via the parameter card and the blocks
which are relevant for the two models used for the experimental
searches are described below. The relevant parameters in the Mad-
Graph parameter cards, also expressed in the notation introduced in
the previous Section, are as follows for the two models considered.

1. Resonant scalar model described by the Lagrangian (5.3)

   • `AQS` and `BQS`: 3×3 matrices (flavour space) fixing the coupling

of the scalar ϕ (S stands for scalar) and *down*-type quarks (Q stands for quarks), previously called a/b_{SR}.

- `A12S` and `B12S`: 3×1 matrices (flavour space) fixing the coupling of the DM candidate χ (where 12 stands for spin-1/2 fermion) and *up*-type quarks, previously called $a_{VR}^{1/2}$.

- particle names: the scalar $\phi^{\pm}$ is labeled S and the fermion χ is f_{met}

2. Non-resonant vectorial model described by the Lagrangian (5.4)

- `A1FC` and `B1FC`: 3×3 matrices (flavour space) fixing the coupling of the vector V (1 stands for vector) and *up*-type quarks, previously called a_{FC}^0.

- particle name: the vector V is labelled v_{met}, while the dark matter candidate χ is not implemented (as this model assumes BR($V \to \chi\chi$) = 100%)

The width of the scalar resonance and of the new vector are set to only the allowed decays in the models, namely a DM candidate and a top quark for the resonant model.

PARAMETER SCAN

The relevant parameters for the resonant model are:

- The mass of the new scalar ϕ;

- The mass of the DM candidate χ;

- The coupling of the new scalar to the DM candidate and top quark a, related to the width of the scalar in the minimal width assumption;

The relevant parameters for the non-resonant model are:

- The mass of the new vector V;

- The mass of the DM candidate χ;

- The coupling of the new vector to the up and top quark a, related to the width of the scalar in the minimal width assumption;

- The coupling of the new vector to the DM candidate χ, related to the branching fraction of the vector into invisible and visible particle, and as a consequence to the width of the vector.

It has been checked for the non-resonant model that the relevant kinematics does not change when changing the width of the resonance. Figures 5.9 and 5.10 show the V mass distribution, the transverse momentum for V and for the top quark from the $V \to t\bar{u}$ decay,
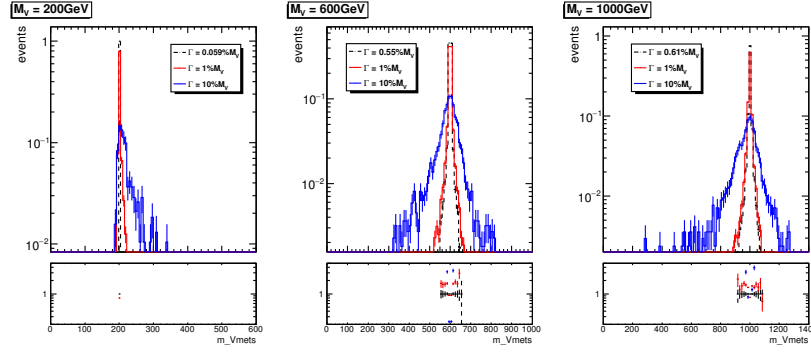
Figure 5.8: Distribution of V invariant mass for the $gu \rightarrow tV(\rightarrow t\bar{u})$ (on-shell V) for m_V = 200, 600, 1000 GeV (from left to right) and for three different visible decay width (computed from Madgraph directly, 1% and 10%).
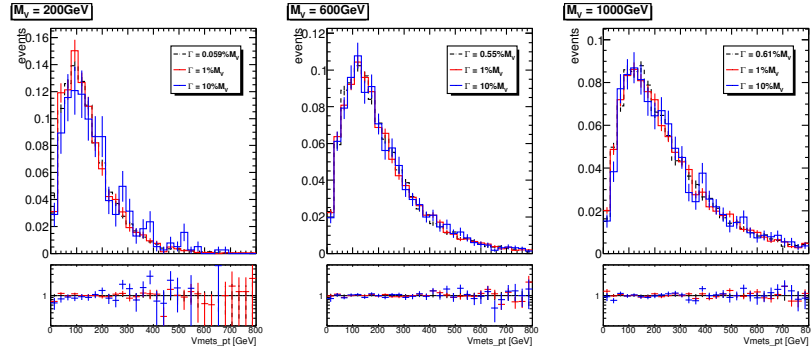
Figure 5.9: Distribution of the V p_T for the $gu \rightarrow tV(\rightarrow t\bar{u})$ (on-shell V) for m_V = 200, 600, 1000 GeV (from left to right) and for three different visible decay width (computed from Madgraph directly, 1% and 10%).
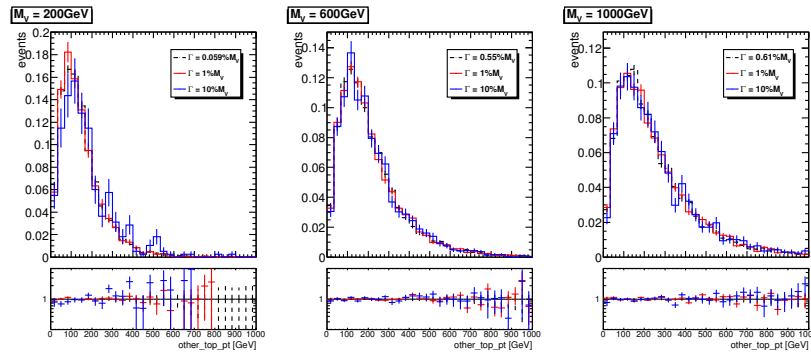
Figure 5.10: Distribution of the top quark p_T produced in association with V in $gu \rightarrow tV$ for m_V = 200, 600, 1000 GeV (from left to right) and for three different visible decay width (computed from Madgraph directly, 1% and 10%).

for different V masses and widths. These figures are relevant independently of the V decay mode (be it visible or invisible).

The limited timescale allowed to reach a consensus for the recommendations contained in this document has not allowed further studies on the parameter scan of these models. The two Collaborations are however encouraged to continue the path started for those studies and agree on a common parameter scan, following the same path as for other models described in this document.

6

Validity of EFT approach

Effective Field Theories (EFTs) are an extremely useful tool for DM searches at the LHC. Given the current lack of indications about the nature of the DM particle and its interactions, a model independent interpretation of the collider bounds appears mandatory, especially in complementarity with the reinterpretation of the exclusion limits within a choice of simplified models, which cannot exhaust the set of possible completions of an effective Lagrangian. However EFTs must be used with caution at LHC energies, where the energy scale of the interaction is at a scale where the EFT approximation can no longer be assumed to be valid. Here we summarise some methods that can be used to ensure the validity of the EFT approximation. These methods are described in detail in Refs. [BDSMR14**?** , BDSJ⁺14, A⁺15, RWZ15].

6.1 *Outline of the procedure described in Refs. [**?** A⁺15]*

For a tree-level interaction between DM and the Standard Model (SM) via some mediator with mass M, the EFT approximation corresponds to expanding the propagator in powers of Q_{tr}^2/M^2, truncating at lowest order, and combining the remaining parameters into a single parameter M_* (also called Λ). For an example scenario with a Z'-type mediator (leading to some combination of operators D5 to D8 in the EFT limit) this corresponds to setting

$$\frac{g_{DM}g_q}{Q_{tr}^2 - M^2} = -\frac{g_{DM}g_q}{M^2}\left(1 + \frac{Q_{tr}^2}{M^2} + \mathcal{O}\left(\frac{Q_{tr}^4}{M^4}\right)\right) \simeq -\frac{1}{M_*^2}, \qquad (6.1)$$

where Q_{tr} is the momentum carried by the mediator, and g_{DM}, g_q are the DM-mediator and quark-mediator couplings respectively. Similar expressions exist for other operators. Clearly the condition that must be satisfied for this approximation to be valid is that $Q_{tr}^2 < M^2 = g_{DM}g_q M_*^2$.

We can use this condition to enforce the validity of the EFT approximation by restricting the signal (after the imposition of the cuts

855 of the analysis) to events for which $Q_{\mathrm{tr}}^2 < M^2$. This truncated sig-
856 nal can then be used to derive the new, truncated limit on M_* as a
857 function of $(m_{\mathrm{DM}}, g_{\mathrm{DM}}g_q)$.

For the example D5-like operator, $\sigma \propto M_*^{-4}$, and so there is a
simple rule for converting a rescaled cross section into a rescaled
constraint on M_* if the original limit is based on a simple cut-and-
count procedure. Defining $\sigma_{\mathrm{EFT}}^{\mathrm{cut}}$ as the cross section truncated such
that all events pass the condition $\sqrt{g_{\mathrm{DM}}g_q}M_*^{\mathrm{rescaled}} > Q_{\mathrm{tr}}$, we have

$$M_*^{\mathrm{rescaled}} = \left(\frac{\sigma_{\mathrm{EFT}}}{\sigma_{\mathrm{EFT}}^{\mathrm{cut}}}\right)^{1/4} M_*^{\mathrm{original}}, \qquad (6.2)$$

858 which can be solved for M_*^{rescaled} via either iteration or a scan (note
859 that M_*^{rescaled} appears on both the LHS and RHS of the equation).
860 Similar relations exist for a given UV completion of each operator.
861 The details and application of this procedure to ATLAS results can be
862 found in Ref. [A$^+$15] for a range of operators. Since this method uses
863 the physical couplings and energy scale Q_{tr}, it gives the strongest
864 possible constraints in the EFT limit while remaining robust by en-
865 suring the validity of the EFT approximation.

6.2 *Outline of the procedure described in Ref. [RWZ15]*

In [RWZ15] a procedure to extract model independent and consistent bounds within the EFT is described. This procedure can be applied to any effective Lagrangian describing the interactions between the DM and the SM, and provides limits that can be directly reinterpreted in any completion of the EFT.

The range of applicability of the EFT is defined by a mass scale M_{cut}, a parameter which marks the upper limit of the range of energy scales at which the EFT can be used reliably, independently of the particular completion of the model. Regardless of the details of the full theory, the energy scale probing the validity of the EFT is less than or equal to the centre-of-mass energy E_{cm}, the total invariant mass of the hard final states of the reaction. Therefore, the condition ensuring the validity of the EFT is, by definition of M_{cut},

$$E_{\text{cm}} < M_{\text{cut}} . \qquad (6.3)$$

For example, in the specific case of a tree level mediation with a single mediator, M_{cut} can be interpreted as the mass of that mediator.

There are then at least three free parameters describing an EFT: the DM mass m_{DM}, the scale M_* of the interaction, and the cutoff scale M_{cut}.

We can use the same technique as above to restrict the signal to the events for which $E_{\text{cm}} < M_{\text{cut}}$, using only these events to derive the exclusion limits on M_* as a function of $(m_{\text{DM}}, M_{\text{cut}})$. We can also define an *effective coupling strength* $M_{\text{cut}} = g_* M_*$, where g_* is a free parameter that substitutes the parameter M_{cut}, and therefore derive exclusions on M_* as a function of (m_{DM}, g_*). This allows us to see how much of the theoretically allowed parameter space has been actually tested and how much is still unexplored; For example, in the Z'-type model considered above, g_* is equal to $\sqrt{g_{\text{DM}} g_q}$. The resulting plots are shown in [RWZ15] for a particular effective operator.

The advantage of this procedure is that the obtained bounds can be directly and easily recast in any completion of the EFT, by computing the parameters M_*, M_{cut} in the full model as functions of the parameters of the complete theory. On the other hand, the resulting limits will be weaker than those obtained using Q_{tr} and a specific UV completion.

A

Appendix: Detailed studies on mono-jet signatures

A.1 CKKW parton matching implementation

The parton matching techniques are implemented in the mono-jet like MC generation in order to avoid double counting the partons from matrix elements and parton showering. The CKKW matching is better developed and preferred in this study. As the illustration sample, the EFT D5 samples are generated with `MadGraph5_aMC@NLO` version 2.2.2. The technical implementations are shown as below.

On the generator side, i.e., `MadGraph5_aMC@NLO`:

- `ickkw = 0`

- `ktdurham = matching scale`

- `dparameter = 0.4`

- `dokt = T`

- `ptj=20`

- `drjj=0`

- `mmjj=0`

- `ptj1min=0`

On the parton showering side, i.e., `Pythia 8`:

- `Merging:ktType = 1`

- `Merging:TMS = matching scale`

- `1000022:all = chi chi  2 0 0 30.0 0.0 0.0 0.0 0.0`

- `1000022:isVisible = false`

- `Merging:doKTMerging = on`

- `Merging:Process = pp>chi,1000022chi ,-1000022`

918 • `Merging:nJetMax = 2`

919 The matching scales should be the same for the generation and par-
920 ton showering. In MadGraph5_aMC@NLO, the particle data group ID
921 `1000022` is used for weakly interacting dark matter candidates, which
922 should be informed to `Pythia 8`.

923 In this test we are generating the process with up to two par-
924 ton emissions, so the command `Merging:nJetMax = 2` is applied to
925 `Pythia 8`. The different parton emission cases are generated sepa-
926 rately:

927 • `p p > chi chi`

928 • `p p > chi chi  j`

929 • `p p > chi chi  j j`

930 Two matching scales are tested at 30 and 80 GeV. The differential jet
931 rates are shown in Fig. A.1 for matching scale 30 GeV and Fig. A.2
932 for 80 GeV. The 80 GeV matching scale gives smoother distribution,
933 which is desired to avoid artifical effect due to parton matching.
934 There will be a small tink around the matching scale for both cases.

(a) 1 → 2 parton process

(b) 2 → 3 parton process

(c) 3 → 4 parton process

(d) 4 → 5 parton process

Figure A.1: Jet differential rates distributions for EFT D5 sample with CKKW matching scale at 30 GeV. 0-, 1- and 2-parton emission cases are generated separatedly.

935 The MC distributions for the missing transverse energy and trans-
936 verse momenta for the leading and subleading jets are plotted in Fig..
937 For the mono-jet analysis, usually a missing transverse energy cut
938 larger than 300 GeV is applied for offline selection, which makes the
939 contribution of the 0-parton emission case negligible in the mono-jet
940 analysis.

(a) $1 \rightarrow 2$ parton process

(b) $2 \rightarrow 3$ parton process

(c) $3 \rightarrow 4$ parton process

(d) $4 \rightarrow 5$ parton process
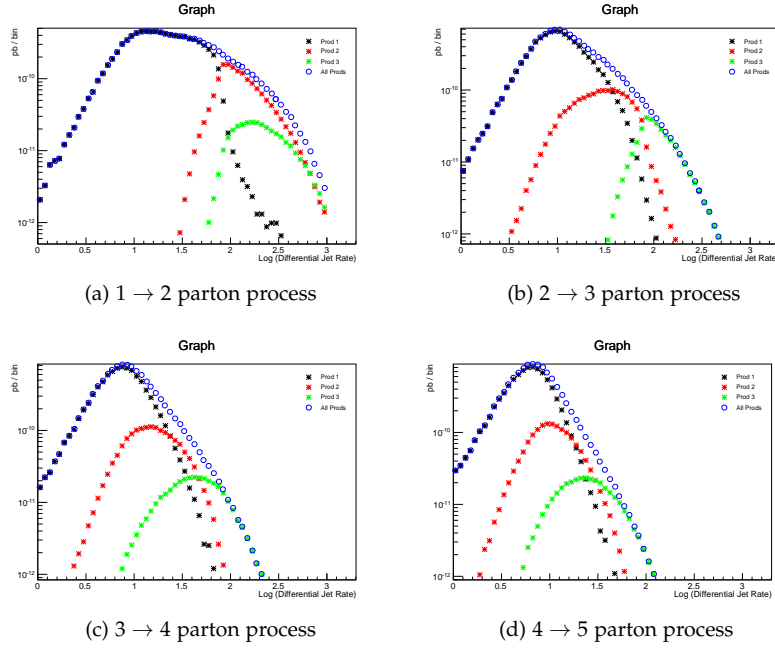
Figure A.2: Jet differential rates distributions for EFT D5 sample with CKKW matching scale at 80 GeV. 0-, 1- and 2-parton emission cases are generated separatedly.

(a) Missing transverse momentum
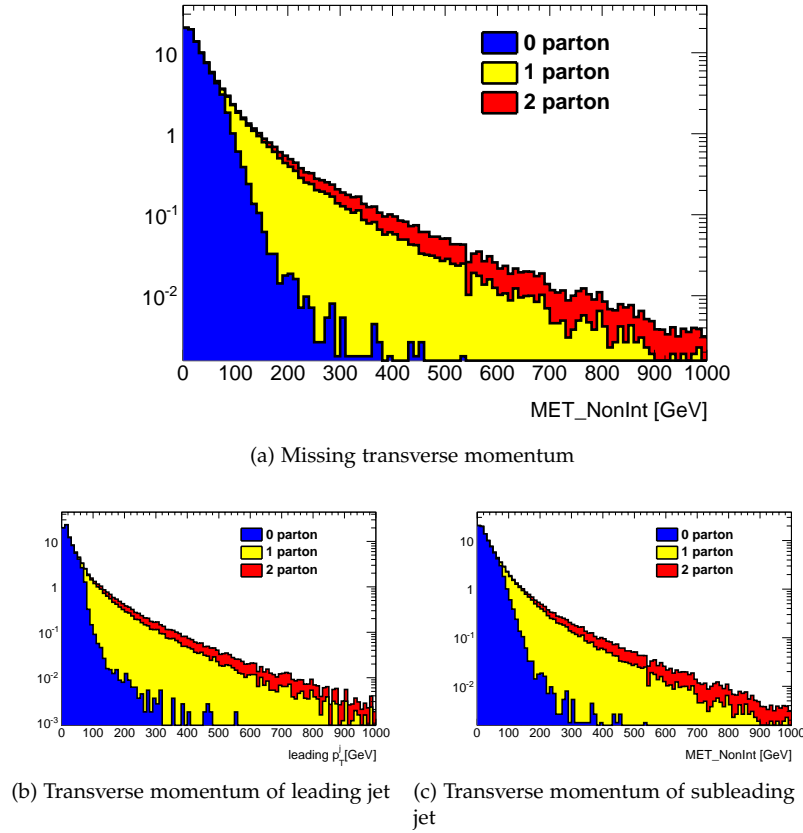
Figure A.3: Kinematics distributions for EFT D5 sample with CKKW matching scale at 80 GeV. 0-, 1- and 2-parton emission cases are generated separatedly and added together by cross sections. The 0-parton emission case has very limited contribution for missing transverse energy larger than 300 GeV region.

(b) Transverse momentum of leading jet

(c) Transverse momentum of subleading jet

A.2   *Parton emission generation*

In order to describe the signal kinematics correctly and save time in MC generation, the parton emissions will only be generated up to a certain numbers of parton and ignore the cases with more partons. The later ones usually have cross sections small enough and limited contribution in the interested kinematic regions.

It is found that the 3- or more-parton emission cases are negligible in our intersted regions, but the 2-parton emission case has significant contributions. The 0- and 1-parton emissions are out of discussion since they give the baseline signature in this analysis. The impacts of 2- and 3-parton emissions are quantified in this section.

Here the 0-, 1-, 2- and 3-parton emissions are generated separately and requested in matching step with `Merging:nJetMax=3` and scale at 80 GeV in Pythia8. The kinematic distributions for MET, leading and subleading jet transverse momenta are plotted in Fig, while the jet multiplicity at different leading jet transverse momentum cuts is shown in Fig.
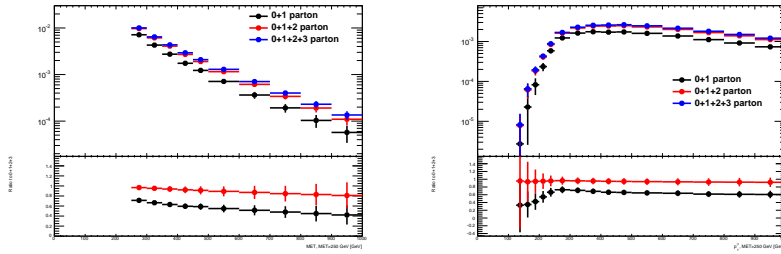
(a) Missing transverse momentum

(b) Transverse momentum of leading jet
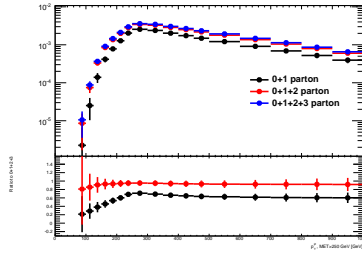
(c) Transverse momentum of subleading jet

Figure A.4: Kinematics distributions for EFT D5 sample with CKKW matching scale at 80 GeV. 0-, 1-, 2- and 3-parton emission cases are generated separatedly and added together by cross sections.

With the ATLAS run-I baseline cut (MET and leading jet p_T larger than 250 GeV, less than 4 jets), the 0+1 parton emission has 11.4% yield less compared to 0+1+2+3 parton emission, while the 0+1+2 has only 0.4% less. With MET>400 GeV, 0+1 parton emission has 16.8% yield less and 0+1+2 parton emission has 0.8% less compared to 0+1+2+3 parton emission. With MET>600 GeV, 0+1 parton emis-
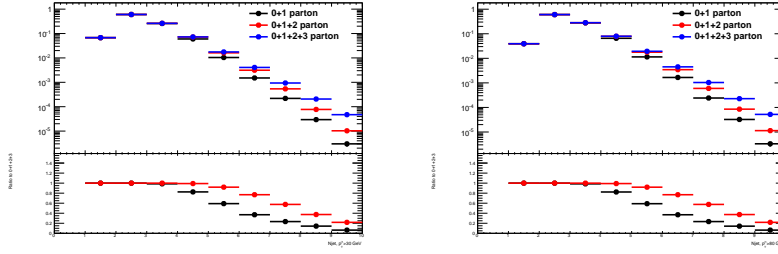
(a) Jet multiplicity, leading jet p_T > 30 GeV

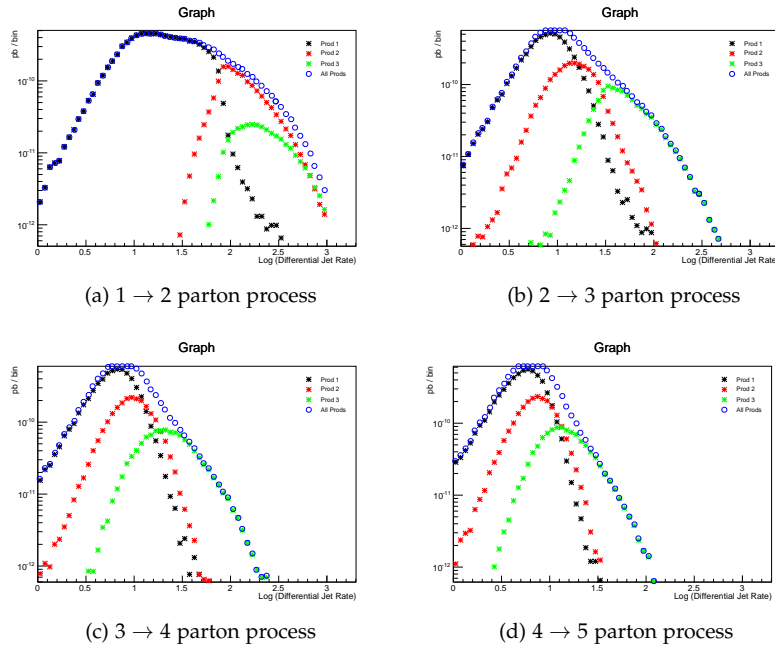(b) Jet multiplicity, leading jet p_T > 80 GeV

Figure A.5: Jet multiplicity distributions for EFT D5 sample with CKKW matching scale at 80 GeV. 0-, 1-, 2- and 3-parton emission cases are generated separatedly and added together by cross sections.
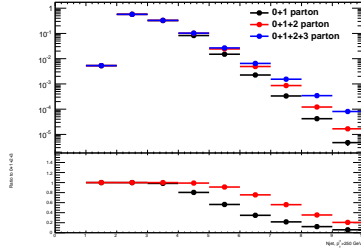
(c) Jet multiplicity, leading jet p_T > 250 GeV

sion has 22.1% yield less and 0+1+2 parton emission has 1.6% less compared to 0+1+2+3 parton emission.

B

Appendix: Detailed studies for EW models

B.1 Further W+MET models with possible cross-section enhancements

As pointed out in Ref. [BCD$^+$15], the mono-*W* signature can probe the iso-spin violating interactions of dark matter with quarks. The relevant operators after the electroweak symmetry breaking is

$$\frac{1}{\Lambda^2}\overline{\chi}\gamma_\mu\chi\left(\overline{u}_L\gamma^\mu u_L + \xi\overline{d}_L\gamma^\mu d_L\right).$$
(B.1)

Here, we only keep the left-handed quarks because the right-handed quarks do not radiate a *W*-gauge boson from the weak interaction. As the LHC constraints the cutoff to higher values, it is also important to know the corresponding operators before the electroweak symmetry. At the dimension-six level, the following operator

$$\frac{c_6}{\Lambda^2}\overline{\chi}\gamma_\mu\chi\,\overline{Q}_L\gamma^\mu Q_L$$
(B.2)

conserves iso-spin and provides us $\xi = 1$ [**?**]. At the dimension-eight level, new operators appear to induce iso-spin violation and can be

$$\frac{c_8^d}{\Lambda^4}\overline{\chi}\gamma_\mu\chi\,(H\overline{Q}_L)\gamma^\mu(Q_L H^\dagger) + \frac{c_8^u}{\Lambda^4}\overline{\chi}\gamma_\mu\chi\,(\tilde{H}\overline{Q}_L)\gamma^\mu(Q_L \tilde{H}^\dagger).$$
(B.3)

After inputting the vacuum expectation value of the Higgs field, we have

$$\xi = \frac{c_6 + c_8^d\,v_{\text{EW}}^2/2\Lambda^2}{c_6 + c_8^u\,v_{\text{EW}}^2/2\Lambda^2}.$$
(B.4)

For a nonzero c_6 and $v_{\text{EW}} \ll \Lambda$, the iso-spin violation effects are suppressed. On the other hand, the values of c_6, c_8^d and c_8^u depend on the UV-models.

There is one possible UV-model to obtain a zero value for c_6 and non-zero values for c_8^d and c_8^u. One can have the dark matter and the SM Higgs field charged under a new $U(1)'$. There is a small mass mixing between SM *Z*-boson and the new *Z'* with a mixing angle

of $\mathcal{O}(v_{\text{EW}}^2/M_{Z'}^2)$. After integrating out Z', one has different effective dark matter couplings to u_L and d_L fields, which are proportional to their couplings to the Z boson. For this model, we have $c_6 = 0$ and

$$\xi = \frac{-\frac{1}{2} + \frac{1}{3}\sin^2\theta_W}{\frac{1}{2} - \frac{2}{3}\sin^2\theta_W} \approx -2.7 \tag{B.5}$$

973   and order of unity.

C

Appendix: Table of cross sections for $t\bar{t}$+MET searches

All tables need to be adjusted with right number of significant digits

Coupling (g)	m_{Phi} [GeV]	m_χ [GeV]	Γ_{min} [GeV]	σ
0.1	10	1	0.00374318	0.207 ± 0.0006846
0.1	20	1	0.00784569	0.1121 ± 0.0003285
0.1	50	1	0.01987	0.03211 ± 0.0001005
0.1	100	1	0.0398141	$0.007325 \pm 2.416e\text{-}05$
0.1	150	1	0.0597437	$0.002396 \pm 7.419e\text{-}06$
0.1	200	1	0.0796724	$0.001018 \pm 3.398e\text{-}06$
0.1	300	1	0.119549	$0.0003394 \pm 1.234e\text{-}06$
0.1	500	1	0.310863	$6.802e\text{-}05 \pm 2.343e\text{-}07$
0.1	1000	1	0.881329	$5.817e\text{-}06 \pm 2.356e\text{-}08$
0.1	1500	1	1.40417	$8.942e\text{-}07 \pm 3.832e\text{-}09$
0.1	10	10	0.000100	$1.007e\text{-}05 \pm 3.761e\text{-}08$
0.1	20	10	0.000100	$3.491e\text{-}05 \pm 1.012e\text{-}07$
0.1	50	10	0.0153395	0.03212 ± 0.0001037
0.1	100	10	0.0374747	$0.007343 \pm 2.011e\text{-}05$
0.1	150	10	0.0581752	$0.002389 \pm 7.654e\text{-}06$
0.1	200	10	0.0784937	$0.001018 \pm 6.258e\text{-}06$
0.1	300	10	0.118762	$0.0003373 \pm 1.448e\text{-}06$
0.1	500	10	0.310391	$6.773e\text{-}05 \pm 2.326e\text{-}07$
0.1	1000	10	0.881093	$5.81e\text{-}06 \pm 2.245e\text{-}08$
0.1	1500	10	1.40401	$8.937e\text{-}07 \pm 4.013e\text{-}09$
0.1	50	50	0.0000233555	$2.581e\text{-}07 \pm 1.214e\text{-}09$
0.1	100	50	0.0000492402	$1.526e\text{-}06 \pm 7.038e\text{-}09$
0.1	150	50	0.0247905	$0.002387 \pm 8.272e\text{-}06$
0.1	200	50	0.051794	$0.00102 \pm 3.216e\text{-}06$
0.1	300	50	0.100226	$0.0003366 \pm 1.393e\text{-}06$
0.1	500	50	0.299052	$6.679e\text{-}05 \pm 2.406e\text{-}07$
0.1	1000	50	0.875378	$5.764e\text{-}06 \pm 2.472e\text{-}08$
0.1	1500	50	1.4002	$8.866e\text{-}07 \pm 3.257e\text{-}09$

Table C.1 – continued from previous page

Coupling (g)	m_{Phi} [GeV]	m_χ [GeV]	Γ_{min} [GeV]	σ
0.1	100	150	0.0000492402	1.246e-08 ± 5.121e-11
0.1	150	150	0.0000765167	1.393e-08 ± 6.653e-11
0.1	200	150	0.000106902	1.693e-08 ± 8.493e-11
0.1	300	150	0.000190543	7.557e-08 ± 2.171e-10
0.1	500	150	0.213784	5.063e-05 ± 1.724e-07
0.1	1000	150	0.828844	5.365e-06 ± 2.028e-08
0.1	1500	150	1.36872	8.603e-07 ± 3.769e-09
0.1	200	300	0.000106902	1.415e-09 ± 5.97e-12
0.1	300	300	0.000190543	1.64e-09 ± 7.878e-12
0.1	500	300	0.111924	3.078e-09 ± 1.482e-11
0.1	1000	300	0.687162	3.828e-06 ± 1.416e-08
0.1	1500	300	1.26683	7.579e-07 ± 3.041e-09
0.1	500	500	0.111924	1.784e-10 ± 1.105e-12
0.1	1000	500	0.483444	1.98e-09 ± 9.199e-12
0.1	1500	500	1.05448	4.92e-07 ± 2.14e-09
0.3	10	1	0.0336886	1.876 ± 0.006611
0.3	20	1	0.0706112	1.006 ± 0.003894
0.3	50	1	0.17883	0.2886 ± 0.0009285
0.3	100	1	0.358327	0.06598 ± 0.000182
0.3	150	1	0.537693	0.0214 ± 6.701e-05
0.3	200	1	0.717052	0.009216 ± 3.533e-05
0.3	300	1	1.07594	0.003044 ± 1.194e-05
0.3	500	1	2.79777	0.0006105 ± 2.187e-06
0.3	1000	1	7.93196	5.256e-05 ± 2.165e-07
0.3	1500	1	12.6376	8.048e-06 ± 3.473e-08
0.3	10	10	5.69808	0.0008143 ± 3.272e-06
0.3	20	10	0.0000630938	0.002836 ± 9.724e-06
0.3	50	10	0.138055	0.2869 ± 0.0008971
0.3	100	10	0.337272	0.06606 ± 0.0002407
0.3	150	10	0.523576	0.02145 ± 8.01e-05
0.3	200	10	0.706443	0.009222 ± 2.807e-05
0.3	300	10	1.06886	0.003051 ± 1.001e-05
0.3	500	10	2.79352	0.0006115 ± 2.268e-06
0.3	1000	10	7.92983	5.24e-05 ± 1.964e-07
0.3	1500	10	12.6361	8.053e-06 ± 3.203e-08
0.3	10	50	5.69808	1.704e-05 ± 7.077e-08
0.3	20	50	0.0000630938	1.746e-05 ± 7.383e-08
0.3	50	50	0.000210199	2.071e-05 ± 8.162e-08
0.3	100	50	0.000443162	0.0001245 ± 3.888e-07
0.3	150	50	0.223114	0.02138 ± 6.22e-05

Table C.1 – continued from previous page

Coupling (g)	m_{Phi} [GeV]	m_χ [GeV]	Γ_{min} [GeV]	σ
0.3	200	50	0.466146	$0.009186 \pm 3.168\text{e-}05$
0.3	300	50	0.902031	$0.003039 \pm 1.09\text{e-}05$
0.3	500	50	2.69146	$0.0005971 \pm 2.181\text{e-}06$
0.3	1000	50	7.8784	$5.222\text{e-}05 \pm 1.907\text{e-}07$
0.3	1500	50	12.6018	$7.947\text{e-}06 \pm 2.996\text{e-}08$
0.3	100	150	0.000443162	$1.004\text{e-}06 \pm 4.682\text{e-}09$
0.3	150	150	0.00068865	$1.132\text{e-}06 \pm 4.644\text{e-}09$
0.3	200	150	0.000962116	$1.349\text{e-}06 \pm 6.834\text{e-}09$
0.3	300	150	0.00171489	$6.08\text{e-}06 \pm 2.289\text{e-}08$
0.3	500	150	1.92405	$0.000456 \pm 2.064\text{e-}06$
0.3	1000	150	7.45959	$4.818\text{e-}05 \pm 1.84\text{e-}07$
0.3	1500	150	12.3185	$7.796\text{e-}06 \pm 2.802\text{e-}08$
0.3	200	300	0.000962116	$1.144\text{e-}07 \pm 4.635\text{e-}10$
0.3	300	300	0.00171489	$1.324\text{e-}07 \pm 6.534\text{e-}10$
0.3	500	300	1.00732	$2.5\text{e-}07 \pm 1.113\text{e-}09$
0.3	1000	300	6.18446	$3.439\text{e-}05 \pm 1.376\text{e-}07$
0.3	1500	300	11.4014	$6.834\text{e-}06 \pm 2.623\text{e-}08$
0.3	500	500	1.00732	$1.449\text{e-}08 \pm 5.536\text{e-}11$
0.3	1000	500	4.35099	$1.487\text{e-}07 \pm 6.617\text{e-}10$
0.3	1500	500	9.49035	$4.374\text{e-}06 \pm 1.739\text{e-}08$
0.7	10	1	0.183416	10.2 ± 0.03649
0.7	20	1	0.384439	5.462 ± 0.02022
0.7	50	1	0.97363	1.558 ± 0.004491
0.7	100	1	1.95089	0.3568 ± 0.001143
0.7	150	1	2.92744	0.1161 ± 0.0003685
0.7	200	1	3.90395	0.04995 ± 0.0001494
0.7	300	1	5.85789	$0.01649 \pm 5.579\text{e-}05$
0.7	500	1	15.2323	$0.003313 \pm 1.464\text{e-}05$
0.7	1000	1	43.1851	$0.0002823 \pm 1.233\text{e-}06$
0.7	1500	1	68.8045	$4.481\text{e-}05 \pm 1.885\text{e-}07$
0.7	10	10	0.0000310229	0.02403 ± 0.0001038
0.7	20	10	0.000343511	0.08347 ± 0.0004742
0.7	50	10	0.751635	1.553 ± 0.004764
0.7	100	10	1.83626	0.3569 ± 0.0009501
0.7	150	10	2.85058	0.1165 ± 0.0004139
0.7	200	10	3.84619	0.04984 ± 0.0001855
0.7	300	10	5.81933	$0.01649 \pm 6.843\text{e-}05$
0.7	500	10	15.2092	$0.003301 \pm 1.289\text{e-}05$
0.7	1000	10	43.1735	$0.0002815 \pm 1.129\text{e-}06$
0.7	1500	10	68.7967	$4.491\text{e-}05 \pm 2.108\text{e-}07$

Table C.1 – continued from previous page

Coupling (g)	m_{Phi} [GeV]	m_χ [GeV]	Γ_{min} [GeV]	σ
0.7	10	50	0.0000310229	$0.000511 \pm 1.977\text{e-}06$
0.7	20	50	0.000343511	$0.0005184 \pm 2.146\text{e-}06$
0.7	50	50	0.00114442	$0.0006176 \pm 3.053\text{e-}06$
0.7	100	50	0.00241277	$0.003681 \pm 1.333\text{e-}05$
0.7	150	50	1.21473	0.1156 ± 0.0003755
0.7	200	50	2.53791	0.04988 ± 0.0001824
0.7	300	50	4.91106	$0.01651 \pm 6.317\text{e-}05$
0.7	500	50	14.6535	$0.003218 \pm 1.523\text{e-}05$
0.7	1000	50	42.8935	$0.0002794 \pm 1.049\text{e-}06$
0.7	1500	50	68.6098	$4.46\text{e-}05 \pm 1.989\text{e-}07$
0.7	100	150	0.00241277	$2.968\text{e-}05 \pm 1.364\text{e-}07$
0.7	150	150	0.00374932	$3.327\text{e-}05 \pm 1.594\text{e-}07$
0.7	200	150	0.00523819	$4.04\text{e-}05 \pm 1.861\text{e-}07$
0.7	300	150	0.00933663	$0.0001787 \pm 7.694\text{e-}07$
0.7	500	150	10.4754	$0.00243 \pm 1.128\text{e-}05$
0.7	1000	150	40.6133	$0.0002573 \pm 1.014\text{e-}06$
0.7	1500	150	67.0675	$4.239\text{e-}05 \pm 1.707\text{e-}07$
0.7	100	300	0.00241277	$3.132\text{e-}06 \pm 1.547\text{e-}08$
0.7	150	300	0.00374932	$3.227\text{e-}06 \pm 1.433\text{e-}08$
0.7	200	300	0.00523819	$3.393\text{e-}06 \pm 1.437\text{e-}08$
0.7	300	300	0.00933663	$3.918\text{e-}06 \pm 1.628\text{e-}08$
0.7	500	300	5.4843	$7.383\text{e-}06 \pm 2.87\text{e-}08$
0.7	1000	300	33.6709	$0.0001801 \pm 7.992\text{e-}07$
0.7	1500	300	62.0745	$3.644\text{e-}05 \pm 1.473\text{e-}07$
0.7	500	500	5.4843	$4.301\text{e-}07 \pm 1.836\text{e-}09$
0.7	1000	500	23.6887	$3.684\text{e-}06 \pm 2.358\text{e-}08$
0.7	1500	500	51.6697	$2.291\text{e-}05 \pm 9.843\text{e-}08$
1.	10	1	0.374318	20.79 ± 0.08102
1.	20	1	0.784569	11.08 ± 0.0396
1.	50	1	1.987	3.146 ± 0.01331
1.	100	1	3.98141	0.7199 ± 0.002775
1.	150	1	5.97437	0.2354 ± 0.0008189
1.	200	1	7.96724	0.1009 ± 0.0003854
1.	300	1	11.9549	0.03369 ± 0.0001155
1.	500	1	31.0863	$0.006652 \pm 2.898\text{e-}05$
1.	1000	1	88.1329	$0.0005705 \pm 2.817\text{e-}06$
1.	1500	1	140.417	$9.244\text{e-}05 \pm 4.273\text{e-}07$
1.	10	10	0.000063312	0.1009 ± 0.00035
1.	20	10	0.000701043	0.3475 ± 0.002265
1.	50	10	1.53395	3.139 ± 0.01028

Table C.1 – continued from previous page

Coupling (g)	m_{Phi} [GeV]	m_χ [GeV]	Γ_{min} [GeV]	σ
1.	100	10	3.74747	0.7158 ± 0.002486
1.	150	10	5.81752	0.236 ± 0.0007591
1.	200	10	7.84937	0.1013 ± 0.0003668
1.	300	10	11.8762	0.03374 ± 0.0001403
1.	500	10	31.0391	$0.006631 \pm 2.585e\text{-}05$
1.	1000	10	88.1093	$0.0005663 \pm 2.515e\text{-}06$
1.	1500	10	140.401	$9.408e\text{-}05 \pm 4.698e\text{-}07$
1.	10	50	0.000063312	$0.00212 \pm 8.815e\text{-}06$
1.	20	50	0.000701043	$0.002149 \pm 9.604e\text{-}06$
1.	50	50	0.00233555	$0.002568 \pm 1.017e\text{-}05$
1.	100	50	0.00492402	$0.01523 \pm 5.043e\text{-}05$
1.	150	50	2.47905	0.2351 ± 0.0008404
1.	200	50	5.1794	0.09993 ± 0.0003164
1.	300	50	10.0226	0.03349 ± 0.0001351
1.	500	50	29.9052	$0.006402 \pm 2.604e\text{-}05$
1.	1000	50	87.5378	$0.0005634 \pm 2.601e\text{-}06$
1.	1500	50	140.02	$9.211e\text{-}05 \pm 4.909e\text{-}07$
1.	100	150	0.00492402	$0.0001247 \pm 5.899e\text{-}07$
1.	150	150	0.00765167	$0.0001387 \pm 5.889e\text{-}07$
1.	200	150	0.0106902	$0.000168 \pm 7.656e\text{-}07$
1.	300	150	0.0190543	$0.0007464 \pm 2.977e\text{-}06$
1.	500	150	21.3784	$0.004856 \pm 1.95e\text{-}05$
1.	1000	150	82.8844	$0.0005122 \pm 1.98e\text{-}06$
1.	1500	150	136.872	$8.662e\text{-}05 \pm 3.821e\text{-}07$
1.	200	300	0.0106902	$1.422e\text{-}05 \pm 6.147e\text{-}08$
1.	300	300	0.0190543	$1.626e\text{-}05 \pm 6.865e\text{-}08$
1.	500	300	11.1924	$3.081e\text{-}05 \pm 1.244e\text{-}07$
1.	1000	300	68.7162	$0.0003534 \pm 1.392e\text{-}06$
1.	1500	300	126.683	$7.258e\text{-}05 \pm 3.651e\text{-}07$
1.	500	500	11.1924	$1.777e\text{-}06 \pm 9.67e\text{-}09$
1.	1000	500	48.3444	$1.331e\text{-}05 \pm 6.551e\text{-}08$
1.	1500	500	105.448	$4.443e\text{-}05 \pm 1.988e\text{-}07$
1.5	10	1	0.842215	46.59 ± 0.1797
1.5	20	1	1.76528	24.52 ± 0.08387
1.5	50	1	4.47075	6.903 ± 0.02244
1.5	100	1	8.95817	1.577 ± 0.005493
1.5	150	1	13.4423	0.5224 ± 0.002309
1.5	200	1	17.9263	0.2259 ± 0.0008625
1.5	300	1	26.8985	0.07529 ± 0.0003407
1.5	500	1	69.9442	$0.01445 \pm 6.469e\text{-}05$

Table C.1 – continued from previous page

Coupling (g)	m_{Phi} [GeV]	m_χ [GeV]	Γ_{min} [GeV]	σ
1.5	1000	1	198.299	$0.001234 \pm 5.694\text{e-}06$
1.5	1500	1	315.939	$0.0002179 \pm 1.024\text{e-}06$
1.5	10	10	0.000142452	0.5117 ± 0.002037
1.5	20	10	0.00157735	1.763 ± 0.01031
1.5	50	10	3.45138	6.906 ± 0.02283
1.5	100	10	8.4318	1.568 ± 0.006489
1.5	150	10	13.0894	0.5162 ± 0.001934
1.5	200	10	17.6611	0.2249 ± 0.0008153
1.5	300	10	26.7214	0.07541 ± 0.0002941
1.5	500	10	69.8379	$0.01447 \pm 6.923\text{e-}05$
1.5	1000	10	198.246	$0.001242 \pm 6.739\text{e-}06$
1.5	1500	10	315.903	$0.0002157 \pm 8.805\text{e-}07$
1.5	10	50	0.000142452	$0.01068 \pm 4.527\text{e-}05$
1.5	20	50	0.00157735	$0.01093 \pm 6.079\text{e-}05$
1.5	50	50	0.00525498	$0.01302 \pm 6.649\text{e-}05$
1.5	100	50	0.011079	0.07677 ± 0.0002445
1.5	150	50	5.57786	0.5195 ± 0.001577
1.5	200	50	11.6536	0.2195 ± 0.0006711
1.5	300	50	22.5508	0.07353 ± 0.0003291
1.5	500	50	67.2866	$0.0139 \pm 6.13\text{e-}05$
1.5	1000	50	196.96	$0.001209 \pm 7.038\text{e-}06$
1.5	1500	50	315.045	$0.0002109 \pm 8.631\text{e-}07$
1.5	100	150	0.011079	$0.0006295 \pm 3.008\text{e-}06$
1.5	150	150	0.0172162	$0.000706 \pm 3.661\text{e-}06$
1.5	200	150	0.0240529	$0.00086 \pm 3.608\text{e-}06$
1.5	300	150	0.0428723	$0.003751 \pm 1.304\text{e-}05$
1.5	500	150	48.1013	$0.01046 \pm 4.013\text{e-}05$
1.5	1000	150	186.49	$0.001072 \pm 4.469\text{e-}06$
1.5	1500	150	307.963	$0.0001931 \pm 1.022\text{e-}06$
1.5	200	300	0.0240529	$7.176\text{e-}05 \pm 3.641\text{e-}07$
1.5	300	300	0.0428723	$8.3\text{e-}05 \pm 3.627\text{e-}07$
1.5	500	300	25.183	$0.000155 \pm 6.658\text{e-}07$
1.5	1000	300	154.611	$0.0007234 \pm 2.773\text{e-}06$
1.5	1500	300	285.036	$0.0001529 \pm 7.694\text{e-}07$
1.5	500	500	25.183	$9.099\text{e-}06 \pm 4.301\text{e-}08$
1.5	1000	500	108.775	$5.335\text{e-}05 \pm 2.699\text{e-}07$
1.5	1500	500	237.259	$8.736\text{e-}05 \pm 4.268\text{e-}07$
2.	10	1	1.49727	82.65 ± 0.3408
2.	20	1	3.13828	43.1 ± 0.1487
2.	50	1	7.948	11.84 ± 0.04278

Continued on next page

Table C.1 – continued from previous page

Coupling (g)	m_{Phi} [GeV]	m_χ [GeV]	Γ_{min} [GeV]	σ
2.	100	1	15.9256	2.712 ± 0.01209
2.	150	1	23.8975	0.9056 ± 0.004237
2.	200	1	31.869	0.3952 ± 0.001653
2.	300	1	47.8195	0.132 ± 0.0004713
2.	500	1	124.345	0.02461 ± 0.0001101
2.	1000	1	352.532	$0.002071 \pm 1.061e\text{-}05$
2.	1500	1	561.669	$0.0003815 \pm 1.4e\text{-}06$
2.	10	10	0.000253248	1.627 ± 0.005672
2.	20	10	0.00280417	5.528 ± 0.03152
2.	50	10	6.13579	11.98 ± 0.04005
2.	100	10	14.9899	2.696 ± 0.01091
2.	150	10	23.2701	0.8981 ± 0.004067
2.	200	10	31.3975	0.3921 ± 0.001675
2.	300	10	47.5047	0.1312 ± 0.0005524
2.	500	10	124.156	0.02454 ± 0.0001302
2.	1000	10	352.437	$0.002051 \pm 9.73e\text{-}06$
2.	1500	10	561.606	$0.0003797 \pm 1.522e\text{-}06$
2.	10	50	0.000253248	0.03397 ± 0.0001354
2.	20	50	0.00280417	0.03452 ± 0.0001623
2.	50	50	0.00934219	0.04088 ± 0.0001623
2.	100	50	0.0196961	0.24 ± 0.0008579
2.	150	50	9.9162	0.8991 ± 0.002903
2.	200	50	20.7176	0.382 ± 0.001411
2.	300	50	40.0903	0.1287 ± 0.0005596
2.	500	50	119.621	0.02328 ± 0.0001255
2.	1000	50	350.151	$0.001995 \pm 1.184e\text{-}05$
2.	1500	50	560.08	$0.0003671 \pm 1.741e\text{-}06$
2.	10	150	0.000253248	$0.001822 \pm 7.946e\text{-}06$
2.	20	150	0.00280417	$0.001842 \pm 8.453e\text{-}06$
2.	50	150	0.00934219	$0.00187 \pm 8.818e\text{-}06$
2.	100	150	0.0196961	$0.001985 \pm 8.101e\text{-}06$
2.	150	150	0.0306067	$0.002231 \pm 1.131e\text{-}05$
2.	200	150	0.0427607	$0.002694 \pm 1.215e\text{-}05$
2.	300	150	0.0762174	$0.01186 \pm 4.862e\text{-}05$
2.	500	150	85.5134	$0.01769 \pm 8.02e\text{-}05$
2.	1000	150	331.538	$0.001716 \pm 7.617e\text{-}06$
2.	1500	150	547.49	$0.0003242 \pm 1.537e\text{-}06$
2.	100	300	0.0196961	$0.0002092 \pm 8.197e\text{-}07$
2.	150	300	0.0306067	$0.0002152 \pm 8.37e\text{-}07$
2.	200	300	0.0427607	$0.0002275 \pm 8.607e\text{-}07$

Table C.1 – continued from previous page

Coupling (g)	m_{Phi} [GeV]	m_χ [GeV]	Γ_{min} [GeV]	σ
2.	300	300	0.0762174	$0.0002609 \pm 1.05\text{e-}06$
2.	500	300	44.7698	$0.0004931 \pm 2.01\text{e-}06$
2.	1000	300	274.865	$0.001119 \pm 5.167\text{e-}06$
2.	1500	300	506.731	$0.0002432 \pm 1.053\text{e-}06$
2.	300	500	0.0762174	$2.367\text{e-}05 \pm 1.206\text{e-}07$
2.	500	500	44.7698	$2.871\text{e-}05 \pm 1.09\text{e-}07$
2.	1000	500	193.378	$0.000131 \pm 5.569\text{e-}07$
2.	1500	500	421.793	$0.0001323 \pm 5.222\text{e-}07$
2.5	10	1	2.33949	128.4 ± 0.4393
2.5	20	1	4.90356	65.92 ± 0.2248
2.5	50	1	12.4187	17.77 ± 0.0663
2.5	100	1	24.8838	4.051 ± 0.01562
2.5	150	1	37.3398	1.364 ± 0.004927
2.5	200	1	49.7953	0.6008 ± 0.002928
2.5	300	1	74.718	0.2036 ± 0.0008994
2.5	500	1	194.29	0.03629 ± 0.0001865
2.5	1000	1	550.831	$0.002918 \pm 1.235\text{e-}05$
2.5	1500	1	877.608	$0.0005639 \pm 2.327\text{e-}06$
2.5	10	10	0.0003957	3.918 ± 0.0159
2.5	20	10	0.00438152	13.54 ± 0.05349
2.5	50	10	9.58718	18.03 ± 0.06068
2.5	100	10	23.4217	4.025 ± 0.01458
2.5	150	10	36.3595	1.36 ± 0.00698
2.5	200	10	49.0586	0.5979 ± 0.002445
2.5	300	10	74.2262	0.2016 ± 0.0006995
2.5	500	10	193.994	0.03579 ± 0.0001738
2.5	1000	10	550.683	$0.002902 \pm 1.515\text{e-}05$
2.5	1500	10	877.509	$0.0005651 \pm 2.275\text{e-}06$
2.5	10	50	0.0003957	0.08298 ± 0.000365
2.5	20	50	0.00438152	0.08474 ± 0.0003631
2.5	50	50	0.0145972	0.09986 ± 0.000455
2.5	100	50	0.0307751	0.5855 ± 0.001667
2.5	150	50	15.4941	1.359 ± 0.005802
2.5	200	50	32.3712	0.5728 ± 0.002188
2.5	300	50	62.6411	0.1938 ± 0.0008665
2.5	500	50	186.907	0.03384 ± 0.0001589
2.5	1000	50	547.111	$0.002773 \pm 1.645\text{e-}05$
2.5	1500	50	875.125	$0.0005349 \pm 3.534\text{e-}06$
2.5	10	150	0.0003957	$0.004461 \pm 1.951\text{e-}05$
2.5	20	150	0.00438152	$0.004473 \pm 2.159\text{e-}05$

Table C.1 – continued from previous page

Coupling (g)	m_{Phi} [GeV]	m_χ [GeV]	Γ_{min} [GeV]	σ
2.5	50	150	0.0145972	$0.00451 \pm 1.808\text{e-}05$
2.5	100	150	0.0307751	$0.00486 \pm 1.984\text{e-}05$
2.5	150	150	0.0478229	$0.00548 \pm 2.35\text{e-}05$
2.5	200	150	0.0668136	$0.006545 \pm 2.81\text{e-}05$
2.5	300	150	0.11909	0.02878 ± 0.0001168
2.5	500	150	133.615	0.02572 ± 0.00011
2.5	1000	150	518.027	$0.002339 \pm 1.101\text{e-}05$
2.5	1500	150	855.453	$0.0004622 \pm 2.297\text{e-}06$
2.5	100	300	0.0307751	$0.0005104 \pm 2.62\text{e-}06$
2.5	150	300	0.0478229	$0.000526 \pm 2.091\text{e-}06$
2.5	200	300	0.0668136	$0.0005503 \pm 2.402\text{e-}06$
2.5	300	300	0.11909	$0.0006368 \pm 2.911\text{e-}06$
2.5	500	300	69.9528	$0.001197 \pm 4.697\text{e-}06$
2.5	1000	300	429.476	$0.001499 \pm 6.445\text{e-}06$
2.5	1500	300	791.767	$0.0003277 \pm 1.439\text{e-}06$
2.5	300	500	0.11909	$5.773\text{e-}05 \pm 2.645\text{e-}07$
2.5	500	500	69.9528	$6.973\text{e-}05 \pm 3.037\text{e-}07$
2.5	1000	500	302.152	$0.0002498 \pm 1.042\text{e-}06$
2.5	1500	500	659.052	$0.000172 \pm 8.531\text{e-}07$
3.	10	1	3.36886	185.9 ± 0.8608
3.	20	1	7.06112	92.49 ± 0.3581
3.	50	1	17.883	24.38 ± 0.08507
3.	100	1	35.8327	5.551 ± 0.02275
3.	150	1	53.7693	1.878 ± 0.008801
3.	200	1	71.7052	0.8398 ± 0.004651
3.	300	1	107.594	0.2856 ± 0.001301
3.	500	1	279.777	0.04861 ± 0.0002143
3.	1000	1	793.196	$0.003716 \pm 1.874\text{e-}05$
3.	1500	1	1263.76	$0.0007294 \pm 3.217\text{e-}06$
3.	10	10	0.000569808	8.181 ± 0.03184
3.	20	10	0.00630938	28.05 ± 0.09412
3.	50	10	13.8055	24.97 ± 0.07128
3.	100	10	33.7272	5.485 ± 0.01916
3.	150	10	52.3576	1.858 ± 0.007406
3.	200	10	70.6443	0.8336 ± 0.003435
3.	300	10	106.886	0.2832 ± 0.001293
3.	500	10	279.352	0.04802 ± 0.0003129
3.	1000	10	792.983	$0.003669 \pm 1.542\text{e-}05$
3.	1500	10	1263.61	$0.0007221 \pm 3.036\text{e-}06$
3.	10	50	0.000569808	0.1714 ± 0.0007653

Continued on next page

Table C.1 – continued from previous page

Coupling (g)	m_{Phi} [GeV]	m_χ [GeV]	Γ_{min} [GeV]	σ
3.	20	50	0.00630938	0.1751 ± 0.000689
3.	50	50	0.0210199	0.2073 ± 0.001019
3.	100	50	0.0443162	1.21 ± 0.003153
3.	150	50	22.3114	1.896 ± 0.007571
3.	200	50	46.6146	0.787 ± 0.002939
3.	300	50	90.2031	0.2685 ± 0.001344
3.	500	50	269.146	0.04468 ± 0.0002221
3.	1000	50	787.84	$0.003505 \pm 1.861\text{e-}05$
3.	1500	50	1260.18	$0.0006823 \pm 3.857\text{e-}06$
3.	10	150	0.000569808	$0.009285 \pm 4.234\text{e-}05$
3.	20	150	0.00630938	$0.00924 \pm 4.234\text{e-}05$
3.	50	150	0.0210199	$0.009462 \pm 3.85\text{e-}05$
3.	100	150	0.0443162	$0.01017 \pm 4.443\text{e-}05$
3.	150	150	0.068865	$0.01124 \pm 5.221\text{e-}05$
3.	200	150	0.0962116	$0.01366 \pm 6.834\text{e-}05$
3.	300	150	0.171489	0.05937 ± 0.0002495
3.	500	150	192.405	0.03448 ± 0.0001467
3.	1000	150	745.959	$0.00288 \pm 1.359\text{e-}05$
3.	1500	150	1231.85	$0.0005735 \pm 3.925\text{e-}06$
3.	50	300	0.0210199	$0.001039 \pm 3.982\text{e-}06$
3.	100	300	0.0443162	$0.001056 \pm 4.834\text{e-}06$
3.	150	300	0.068865	$0.001096 \pm 4.922\text{e-}06$
3.	200	300	0.0962116	$0.001147 \pm 5.869\text{e-}06$
3.	300	300	0.171489	$0.001327 \pm 6.728\text{e-}06$
3.	500	300	100.732	$0.00245 \pm 9.636\text{e-}06$
3.	1000	300	618.446	$0.001853 \pm 7.863\text{e-}06$
3.	1500	300	1140.14	$0.0003934 \pm 2.083\text{e-}06$
3.	150	500	0.068865	$0.0001123 \pm 4.327\text{e-}07$
3.	200	500	0.0962116	$0.000114 \pm 5.127\text{e-}07$
3.	300	500	0.171489	$0.0001206 \pm 5.124\text{e-}07$
3.	500	500	100.732	$0.0001447 \pm 6.102\text{e-}07$
3.	1000	500	435.099	$0.0004016 \pm 1.656\text{e-}06$
3.	1500	500	949.035	$0.0002061 \pm 8.548\text{e-}07$
3.5	10	1	4.58539	257.5 ± 0.9241
3.5	20	1	9.61097	123.8 ± 0.4645
3.5	50	1	24.3407	31.59 ± 0.09614
3.5	100	1	48.7723	7.04 ± 0.02954
3.5	150	1	73.186	2.417 ± 0.01038
3.5	200	1	97.5987	1.089 ± 0.004308
3.5	300	1	146.447	0.3709 ± 0.001616

Table C.1 – continued from previous page

Coupling (g)	m_{Phi} [GeV]	m_χ [GeV]	Γ_{min} [GeV]	σ
3.5	500	1	380.808	0.06035 ± 0.0003762
3.5	1000	1	1079.63	$0.004345 \pm 2.711\text{e-}05$
3.5	1500	1	1720.11	$0.0008581 \pm 3.653\text{e-}06$
3.5	10	10	0.000775572	15.08 ± 0.0569
3.5	20	10	0.00858777	51.42 ± 0.1478
3.5	50	10	18.7909	32.56 ± 0.1113
3.5	100	10	45.9065	6.963 ± 0.03199
3.5	150	10	71.2646	2.38 ± 0.009493
3.5	200	10	96.1548	1.079 ± 0.004244
3.5	300	10	145.483	0.369 ± 0.001602
3.5	500	10	380.229	0.05978 ± 0.0003017
3.5	1000	10	1079.34	$0.004302 \pm 2.412\text{e-}05$
3.5	1500	10	1719.92	$0.0008525 \pm 3.878\text{e-}06$
3.5	10	50	0.000775572	0.3176 ± 0.001314
3.5	20	50	0.00858777	0.3229 ± 0.001215
3.5	50	50	0.0286105	0.3857 ± 0.001618
3.5	100	50	0.0603192	2.228 ± 0.00751
3.5	150	50	30.3684	2.477 ± 0.008787
3.5	200	50	63.4476	1.025 ± 0.003864
3.5	300	50	122.776	0.3483 ± 0.001614
3.5	500	50	366.338	0.05534 ± 0.0003035
3.5	1000	50	1072.34	$0.004076 \pm 2.371\text{e-}05$
3.5	1500	50	1715.24	$0.0008077 \pm 4.889\text{e-}06$
3.5	10	150	0.000775572	$0.01719 \pm 9.115\text{e-}05$
3.5	20	150	0.00858777	$0.01719 \pm 8.334\text{e-}05$
3.5	50	150	0.0286105	$0.01754 \pm 8.239\text{e-}05$
3.5	100	150	0.0603192	$0.01855 \pm 8.371\text{e-}05$
3.5	150	150	0.0937329	0.02099 ± 0.0001038
3.5	200	150	0.130955	0.0252 ± 0.0001138
3.5	300	150	0.233416	0.1096 ± 0.0006465
3.5	500	150	261.885	0.04374 ± 0.0002091
3.5	1000	150	1015.33	$0.00334 \pm 1.751\text{e-}05$
3.5	1500	150	1676.69	$0.0006583 \pm 3.614\text{e-}06$
3.5	10	300	0.000775572	$0.001925 \pm 9.279\text{e-}06$
3.5	20	300	0.00858777	$0.001916 \pm 1.026\text{e-}05$
3.5	50	300	0.0286105	$0.001918 \pm 8.166\text{e-}06$
3.5	100	300	0.0603192	$0.001958 \pm 7.426\text{e-}06$
3.5	150	300	0.0937329	$0.002036 \pm 8.81\text{e-}06$
3.5	200	300	0.130955	$0.002123 \pm 8.379\text{e-}06$
3.5	300	300	0.233416	$0.002448 \pm 9.259\text{e-}06$

Table C.1 – continued from previous page

Coupling (g)	m_{Phi} [GeV]	m_χ [GeV]	Γ_{min} [GeV]	σ
3.5	500	300	137.107	$0.004413 \pm 2.588\text{e-}05$
3.5	1000	300	841.774	$0.002184 \pm 1.014\text{e-}05$
3.5	1500	300	1551.86	$0.0004471 \pm 2.349\text{e-}06$
3.5	10	500	0.000775572	$0.0002016 \pm 7.906\text{e-}07$
3.5	20	500	0.00858777	$0.0002011 \pm 9.138\text{e-}07$
3.5	50	500	0.0286105	$0.0002018 \pm 9.929\text{e-}07$
3.5	100	500	0.0603192	$0.0002033 \pm 8.104\text{e-}07$
3.5	150	500	0.0937329	$0.0002067 \pm 8.026\text{e-}07$
3.5	200	500	0.130955	$0.0002106 \pm 8.439\text{e-}07$
3.5	300	500	0.233416	$0.0002225 \pm 9.256\text{e-}07$
3.5	500	500	137.107	$0.0002686 \pm 1.162\text{e-}06$
3.5	1000	500	592.219	$0.0005877 \pm 2.823\text{e-}06$
3.5	1500	500	1291.74	$0.0002318 \pm 1.11\text{e-}06$

Bibliography

[A$^+$14a] Georges Aad et al. Search for new particles in events with one lepton and missing transverse momentum in pp collisions at $\sqrt{s}$ = 8 TeV with the ATLAS detector. *JHEP*, 1409:037, 2014.

[A$^+$14b] Jalal Abdallah et al. Simplified Models for Dark Matter and Missing Energy Searches at the LHC. *arXiv:1409.2893*, 2014.

[A$^+$15] Georges Aad et al. Search for new phenomena in final states with an energetic jet and large missing transverse momentum in pp collisions at $\sqrt{s}$ = 8 TeV with the ATLAS detector. 2015.

[AAB$^+$14] Jean-Laurent Agram, Jeremy Andrea, Michael Buttignol, Eric Conte, and Benjamin Fuks. Monotop phenomenology at the Large Hadron Collider. *Phys.Rev.*, D89(1):014028, 2014.

[Aad14a] Search for dark matter in events with a hadronically decaying W or Z boson and missing transverse momentum in pp collisions at $\sqrt{s}$ = 8 TeV with the ATLAS detector. *Phys.Rev.Lett.*, 112(4):041802, 2014.

[Aad14b] Search for dark matter in events with a Z boson and missing transverse momentum in pp collisions at $\sqrt{s}$=8 TeV with the ATLAS detector. *Phys.Rev.*, D90(1):012004, 2014.

[Aad15] Search for new phenomena in events with a photon and missing transverse momentum in pp collisions at $\sqrt{s}$ = 8 TeV with the ATLAS detector. *Phys.Rev.*, D91(1):012008, 2015.

[ADR$^+$14] Mohammad Abdullah, Anthony DiFranzo, Arvind Rajaraman, Tim M.P. Tait, Philip Tanedo, et al. Hidden on-shell mediators for the Galactic Center γ-ray excess. *Phys.Rev.*, D90(3):035004, 2014.

[AFM11] J. Andrea, B. Fuks, and F. Maltoni. Monotops at the LHC. *Phys.Rev.*, D84:074025, 2011.

[ATL14] Sensitivity to WIMP Dark Matter in the Final States Containing Jets and Missing Transverse Momentum with the ATLAS Detector at 14 TeV LHC. Technical Report ATL-PHYS-PUB-2014-007, CERN, Geneva, Jun 2014.

[AWZ14] Haipeng An, Lian-Tao Wang, and Hao Zhang. Dark matter with t-channel mediator: a simple step beyond contact interaction. *Phys. Rev. D*, 89:115014, 2014.

[BB13] Yang Bai and Joshua Berger. Fermion Portal Dark Matter. *JHEP*, 11:171, 2013.

[BCD$^+$15] Nicole F. Bell, Yi Cai, James B. Dent, Rebecca K. Leane, and Thomas J. Weiler. Dark matter at the LHC: EFTs and gauge invariance. 2015.

[BCDF15] Idir Boucheneb, Giacomo Cacciapaglia, Aldo Deandrea, and Benjamin Fuks. Revisiting monotop production at the LHC. *JHEP*, 1501:017, 2015.

[BDSJ$^+$14] Giorgio Busoni, Andrea De Simone, Thomas Jacques, Enrico Morgante, and Antonio Riotto. On the Validity of the Effective Field Theory for Dark Matter Searches at the LHC Part III: Analysis for the t-channel. *JCAP*, 1409:022, 2014.

[BDSMR14] Giorgio Busoni, Andrea De Simone, Enrico Morgante, and Antonio Riotto. On the Validity of the Effective Field Theory for Dark Matter Searches at the LHC. *Phys.Lett.*, B728:412–421, 2014.

[BFG15] Matthew R. Buckley, David Feld, and Dorival Goncalves. Scalar Simplified Models for Dark Matter. *Phys.Rev.*, D91(1):015017, 2015.

[BT13] Yang Bai and Tim M.P. Tait. Searches with Mono-Leptons. *Phys.Lett.*, B723:384–387, 2013.

[CDM$^+$14] Linda Carpenter, Anthony DiFranzo, Michael Mulhearn, Chase Shimmin, Sean Tulin, et al. Mono-Higgs-boson: A new collider probe of dark matter. *Phys.Rev.*, D89(7):075017, 2014.

[CEHL14] Spencer Chang, Ralph Edezhath, Jeffrey Hutchinson, and Markus Luty. Effective WIMPs. *Phys. Rev. D*, 89:015011, 2014.

[CHH15]   Andreas Crivellin, Ulrich Haisch, and Anthony Hibbs. LHC constraints on gauge boson couplings to dark matter. 2015.

[CHLR13]   R.C. Cotta, J.L. Hewett, M.P. Le, and T.G. Rizzo. Bounds on Dark Matter Interactions with Electroweak Gauge Bosons. *Phys.Rev.*, D88:116009, 2013.

[CNS+13]   Linda M. Carpenter, Andrew Nelson, Chase Shimmin, Tim M.P. Tait, and Daniel Whiteson. Collider searches for dark matter in events with a Z boson and missing energy. *Phys.Rev.*, D87(7):074005, 2013.

[CRTW14]   Randel C. Cotta, Arvind Rajaraman, Tim M. P. Tait, and Alexander M. Wijangco. Particle Physics Implications and Constraints on Dark Matter Interpretations of the CDMS Signal. *Phys.Rev.*, D90(1):013020, 2014.

[DNRT13]   Anthony DiFranzo, Keiko I. Nagao, Arvind Rajaraman, and Tim M. P. Tait. Simplified Models for Dark Matter Interacting With Quarks. *JHEP*, 1311, 2013.

[Fuk]   Benjamin Fuks. Monotop Effective Theory: MadGraph model. `http://feynrules.irmp.ucl.ac.be/wiki/Monotops`.

[GIR+10]   Jessica Goodman, Masahiro Ibe, Arvind Rajaraman, William Shepherd, Tim M.P. Tait, et al. Constraints on Dark Matter from Colliders. *Phys.Rev.*, D82:116010, 2010.

[HK11]   Robert M. Harris and Konstantinos Kousouris. Searches for dijet resonances at hadron colliders. *Int. J. Modern Phys.*, 26(30n31):5005–5055, 2011.

[HKR13]   Ulrich Haisch, Felix Kahlhoefer, and Emanuele Re. QCD effects in mono-jet searches for dark matter. *JHEP*, 1312:007, 2013.

[HR15]   Ulrich Haisch and Emanuele Re. Simplified dark matter top-quark interactions at the LHC. 2015.

[K+14]   Vardan Khachatryan et al. Search for physics beyond the standard model in final states with a lepton and missing transverse energy in proton-proton collisions at $\sqrt{s} = 8$ TeV. 2014.

[Kha14]   Search for new phenomena in monophoton final states in proton-proton collisions at $\sqrt{s} = 8$ TeV. 2014.

[NCC⁺14] Andy Nelson, Linda M. Carpenter, Randel Cotta, Adam Johnstone, and Daniel Whiteson. Confronting the Fermi Line with LHC data: an Effective Theory of Dark Matter Interaction with Photons. *Phys.Rev.*, D89(5):056011, 2014.

[PVZ14] Michele Papucci, Alessandro Vichi, and Kathryn M. Zurek. Monojet versus the rest of the world I: t-channel models. *JHEP*, 2014.

[RWZ15] Davide Racco, Andrea Wulzer, and Fabio Zwirner. Robust collider limits on heavy-mediator Dark Matter. 2015.

[ZBW13] Ning Zhou, David Berge, and Daniel Whiteson. Mono-everything: combined limits on dark matter production at colliders from multiple final states. *Phys.Rev.*, D87(9):095013, 2013.